

Cosmological Simulations of Elliptical Galaxy Formation in Λ CDM and Λ WDM Cosmologies.

Lisa J. Wright¹, Jeremiah P. Ostriker^{1,2}, Thorsten Naab¹ & George Efstathiou¹

1. *Institute of Astronomy, Madingley Road, Cambridge CB3 0HA, UK*

2. *Department of Astrophysics, Peyton Hall, Princeton, USA*

Accepted ???. Received ???; in original form 7 May 2019

ABSTRACT

We present the results of a series of gas dynamical cosmological simulations of the formation of individual massive field galaxies in the standard concordance Λ CDM and in a Λ WDM cosmology each with $\Omega_0=0.3$ and $\Lambda_0=0.7$. Two high resolution simulations (2×50^3 gas and dark matter particles) have been performed and investigated in detail. The gas component was represented by Smooth Particle Hydrodynamics (SPH) and a simple star formation algorithm was applied. The galaxies form in an initial burst of star formation followed by accretion of small satellites. They do not experience a major merger. The simulated galaxies are old (≈ 10 Gyr) hot stellar systems with masses of $\approx 1.7 \times 10^{11} M_\odot$. Baryonic matter dominates the mass in the luminous part of the galaxies up to ≈ 5 effective radii. The projected properties of the galaxies have been investigated in detail: The Λ CDM galaxy is a slowly rotating ($(v/\sigma)_{\max} = 0.2$) spheroidal stellar system (E2) with predominantly disk isophotes. The line-of-sight velocity distributions (LOSVDs) deviate from Gaussian shape and h_3 is anticorrelated with v_{los} . The corresponding Λ WDM galaxy is more elongated (E3 - E4) and rotates faster ($(v/\sigma)_{\max} = 0.6$). The anisotropy parameter $(v/\sigma)^*$ is close to unity indicating isotropic velocity dispersions. There is no clear indication for isophotal deviations from elliptical shape and the projected LOSVDs do not show correlated higher order deviations from Gaussian shape. Within the uncertainties of M/L both galaxies follow the Fundamental Plane. We conclude that the properties of the two galaxies simulated in the Λ CDM and Λ WDM cosmology are in good agreement with observations of intermediate mass elliptical or S0 galaxies. Our conclusion differs from Meza et al. (2003), who find, from a similar simulation, a much more concentrated galaxy than is generally observed. The differences in our findings may either be the result of differences in the star formation algorithms or due to the different merger history of the galaxies.

Key words:

1 INTRODUCTION

The concordance Λ CDM paradigm (a cold dark matter cosmology with the addition of a cosmological constant) appears to provide an excellent fit to astronomical observations on scales large compared to the sizes of individual galaxies (Percival et al. 2002; Spergel et al. 2003). However there are some indications that the standard model may have too much power on small scales to be consistent with observations. For example, Klypin et al. (1999) show that numerical simulations predict a larger number of Galactic satellites than observed, though Benson et al. (2002) argue that this problem can be solved by the suppression of dwarf galaxy formation in a photoionized inter-galactic medium. A sec-

ond problem relates to the steep cusps found in the centres of simulated dark matter halos (see Moore et al. 1999; Eke et al. 2001; Binney & Evans 2001), which appear to be inconsistent with the dark matter distributions inferred in dwarf galaxies (see *e.g.* Dutton et al. 2003). It is not yet clear whether this discrepancy requires a revision of the Λ CDM model. For example, Ricotti (2003) argues that low mass haloes in the CDM model may have less cuspy profiles than higher mass haloes, though this result is disputed by Colin et al. (2003).

It is also not yet clear whether the properties of real galaxies can be explained by the Λ CDM model. Does the concordance model produce galaxies of the right masses and sizes at the right epochs? In fact there are some indica-

tions from galaxy formation that the concordance model may have too much small scale power. For example, it has proved difficult to make realistic disk galaxies in numerical simulations of the CDM model incorporating gas dynamics. In most simulations, the disk systems that form are smaller, denser and have much lower angular momenta than real disk systems (see Navarro & White 1994, Navarro et al. 1995; Navarro & Steinmetz 1997, Steinmetz & Navarro 1999; Wright 2002). More acceptable fits to real disk systems can be found if heuristic prescriptions modelling stellar feedback are included in the simulations (Weil et al. 1998, Sommer-Larsen et al. 2002, Governato et al. 2002, Abadi et al. 2003). However, even in these simulations, the disk systems typically contain denser and more massive bulges than the vast majority of real disk galaxies.

Most of the previous work on the formation of individual galaxies from cosmological initial conditions has focused on the formation of disk galaxies. The formation of individual elliptical galaxies has not been investigated as extensively. This seems surprising as giant elliptical galaxies are the oldest and most massive stellar systems in the Universe and probably contribute over 50% of the total stellar mass if we include the stars in the bulges of S0, Sa and Sb spirals. Although their internal kinematics can be very complex the major component of the stellar population in ellipticals is old and homogeneous. They are therefore good probes of galaxy assembly, star formation and metal enrichment in the early universe (see e.g. Thomas et al. 2002). Furthermore, the giant ellipticals follow simple scaling relations, the Fundamental Plane being the most important (see e.g. Bender et al. 1992). These simple scaling relations should arise naturally from the correct cosmological model.

Despite their complex kinematics, it has become evident over the last 15 years that observed giant ellipticals show detailed photometric and kinematic properties that correlate with their luminosity. Massive giant ellipticals are slowly rotating, flattened by anisotropic velocity dispersions and show predominantly boxy isophotes. Lower mass giant ellipticals have disk isophotes and are flattened by rotation (Bender et al. 1988). These low mass ellipticals most likely contain weak disk components (Rix & White 1990). The fact that boxy ellipticals, in contrast to disk ellipticals, show strong radio and X-ray emission (Bender et al. 1989) and have flat density cores (Faber et al. 1997) might indicate that they formed either by a different process or in a different environment.

How and when giant ellipticals have formed is still poorly understood. According to the “merger hypothesis” early type galaxies formed by mergers of disk galaxies. Idealised models of binary mergers of disk galaxies (with and without gas and star formation) and multiple mergers have been investigated in great detail by several authors (e.g. Negroponte & White 1983; Hernquist 1992; Barnes 1988; Barnes & Hernquist 1996; Mihos & Hernquist 1996; Weil & Hernquist 1996; Springel 2000). Those simulations – the recent ones with high numerical resolution – are useful in understanding detailed internal processes e.g. gas inflow to the centre (Mihos & Hernquist 1996). They are also capable of explaining the origin of fine structure in individual ellipticals. For example, a large study of collisionless disk mergers by Naab & Burkert (2003) showed that binary disk mergers can successfully reproduce global kinematic and photomet-

ric properties of low and intermediate mass giant ellipticals. The formation of faint embedded disks that are observed in these galaxies can be explained if gas was present in progenitor galaxies (Naab & Burkert 2001a,b; Barnes 2002).

Despite these successes, binary merger simulations suffer from certain limitations. In particular they use approximate equilibrium models of *present day* spiral galaxies as progenitors rather than self-consistently calculating the properties of the progenitors “*ab initio*” from realistic cosmological initial conditions. This is a serious limitation, since it is unlikely that the high redshift progenitors of ellipticals really resembled present day spirals. Added to the model uncertainties there are also a large number of degrees of freedom in the initial conditions, e.g. the geometries of the orbits, halo profiles, bulge masses, bulge rotation, gas content, gas distribution, disk sizes *etc.* are all adjustable parameters. Although there have been attempts to survey e.g. different halo profiles (Dubinski et al. 1996) or disk spin orientations (Naab & Burkert 2003), these parameter surveys are evidently incomplete. In addition, questions regarding a self consistent evolution of stellar populations are extremely difficult to address. Specifically current generation ellipticals are far too red, metal rich and old to have formed via mergers of systems similar to current epoch spirals. Merger simulations have therefore failed, so far, to explain the origin of global scaling relations like the color-magnitude relation or, more generally, the fundamental plane. They have, however, proved very useful in developing an understanding of the detailed internal merger dynamics.

The best way to overcome these problems is via high resolution simulations of individual elliptical galaxies from realistic cosmological initial conditions. The initial conditions are constrained by the cosmological model alone and the subsequent evolution is governed solely by the numerical resolution and accuracy of the physics that is implemented in the simulation. Once a sufficient number of individual ellipticals over the whole mass spectrum have been simulated, it should be possible (if the cosmological model is correct) to explain the origin of the global scaling relations and the detailed properties of individual galaxies at different luminosities.

A first attempt in this direction has been made by Meza et al. 2003. These authors followed the formation of a single spheroidal galaxy in a Λ CDM cosmology. The kinematic properties of their galaxy resembled a rotationally supported giant elliptical. However, the effective radius of the simulated galaxy was a factor of 10 smaller than for observed ellipticals at the same brightness. This galaxy is therefore much too compact to be consistent with observations.

Does this result imply a problem in forming elliptical systems in the Λ CDM model? Two lines of investigation are suggested. First, the cosmological model adopted may be correct but the physical treatment may be inaccurate. Specifically, feedback from some early star formation into the shallow potential wells in the small halos existent at those times, may so efficiently blow out other gas as to reduce early star formation effectively (Dekel & Silk 1986, Efstathiou 2000, Springel & Hernquist 2003 and Nagamine, Cen and Ostriker (in preparation) are also exploring this possibility). The inclusion of stellar feedback would reduce the number of low mass galaxies, but not the number of low mass halos. It would also significantly reduce the stellar

density in the centres of systems, but would not reduce the dark matter density by very much¹.

If, however, it is not obvious that the discrepancy found by Meza et al. 2003 can be cured by a better treatment of the physics. If the evidence for low dark matter densities in the centres of galaxies is taken seriously (Binney & Evans 2001), then we may want to consider a more radical solution.

An alternative is to reduce the small scale power in the dark matter density fluctuations. This can be achieved in various ways. First, the spectral index, n , could be sufficiently small so that after normalization to the WMAP amplitude, and extrapolation to the small wavelengths relevant to galaxy formation, the amplitude is low enough to significantly reduce early star formation. The WMAP analysis (Spergel et al. 2003) combined with 2dFRGS and supernova data in fact indicated that n may be as small as 0.93 ± 0.03 , and this may alleviate some of the purported difficulties of the concordance Λ CDM model. We will return to this possibility in later work. However, there are significant limits on the value of the spectral index n , since information on the cluster length scale ($\sim 8h^{-1} \text{ Mpc}$), which is intermediate between the WMAP scale and the galaxy formation scale seems to require a relatively high normalization (Bahcall et al. 2002). This would not permit a constant n solution with n much less than 0.95. Furthermore, the high optical depth for electron scattering becomes very difficult to achieve with a low spectral index (Cen 2003; Chiu et al. 2003).

Another possibility is to achieve low power on small scales by some form of cut-off in the power spectrum. An example of this is the Warm Dark Matter model, where a finite but quite small initial “thermal” velocity dispersion sharply truncates the power as $(k/k_{\text{cut}})^{-10}$ above some wave number scale, k_{cut} . Bode, Ostriker & Turok (2001) show that

$$k_{\text{cut}} = 17.94 \left(\frac{\Omega_x}{0.3} \right)^{0.15} \times \left(\frac{h}{0.65} \right)^{-1.3} \left(\frac{keV}{m_x} \right)^{-1.15} h \text{ Mpc}^{-1}, \quad (1)$$

where the warm dark matter particle has mass, m_x and the density in WDM is represented by Ω_x , at $z = 0$. The additional velocity dispersions are distributed as

$$f(v) = (e^{v/v_0} + 1)^{-1} \quad (2a)$$

with

$$v_0 = 0.012(1+z) \left(\frac{\Omega_x}{0.3} \right)^{\frac{1}{3}} \left(\frac{h}{0.65} \right)^{\frac{2}{3}} \left(\frac{keV}{m_x} \right)^{\frac{4}{3}} \text{ km/s}. \quad (2b)$$

Barkana, Haiman & Ostriker (2001) used the abundance of small column density lines in the Lyman alpha forest to limit $m_x \gtrsim 0.75 \text{ keV}$. Other work suggests similar limits of $m_x \gtrsim 1 \text{ keV}$, hence, in this paper, we will investigate WDM with $m_x = 1 \text{ keV}$.

One may ask at this point if the WMAP observations

of a high optical depth to the surface of last scattering, τ_{es} , rule out WDM? The answer is ambiguous. An examination of Fig. 5 of Spergel et al. (2003) indicates for $n = 0.95$, τ_{es} may be 0.05 at 1σ level and as small as 0.01 at the 2σ level. Further work is needed (but see Yoshida et al. 2003 for a counter argument) to set a limit on m_x based on WMAP. Detailed work in progress by Ricotti & Ostriker (2003) indicates that, if other parameters are held constant, a WDM model with $m_x = 1.25 \text{ KeV}$ leads to only a $\sim 10\%$ reduction in τ_{es} .

In this paper we aim to investigate formation and evolution of intermediate mass giant galaxies in the Λ CDM model, and to quantify the effect of reducing the power at small scales by studying a Λ WDM model. The paper is organised as follows: Section 2, summarizes the simulation code and describes how Λ CDM and Λ WDM initial conditions were generated. The results of two high resolution simulations in the Λ WDM and Λ CDM universe and a comparison of their global properties with a set of low resolution simulations are described in Section 3. In Section 4 we compare the internal properties of the two high resolution simulations in detail with observations of giant elliptical galaxies. Section 5 contains a summary and our conclusions.

2 INITIAL CONDITIONS AND SIMULATIONS

We performed two sets of cosmological simulations using Λ CDM and Λ WDM initial conditions: 5 simulations with 2×34^3 gas and dark matter particles and 1 simulation with 2×50^3 gas and dark matter particles. The lower resolution simulations were used to investigate the differences in the global properties of the stellar systems formed in each cosmology. The higher resolution simulations were used to investigate the internal properties of the simulated galaxies.

2.1 Power Spectra & Cosmological Parameters

The initial conditions of the Λ CDM and Λ WDM simulations assumed scale-invariant adiabatic fluctuations. The post-recombination power spectrum for both cosmologies is based on the parameterisation of Efstathiou, Bond & White (1992) with $\Gamma=0.2$ and the transfer function

$$T(k) = \frac{1}{\{1 + [ak + (bk)^{3/2} + (ck)^2]^\nu\}^{1/\nu}}, \quad (3a)$$

where

$$a = \left(\frac{6.4}{\Gamma} \right), \quad b = \left(\frac{3.0}{\Gamma} \right), \quad c = \left(\frac{1.7}{\Gamma} \right) \quad (3b)$$

with units of $h^{-1} \text{ Mpc}$ and

$$\nu = 1.13 \quad \text{and} \quad \Gamma = 0.2. \quad (3c)$$

The power spectrum of the dark matter fluctuations in the Λ CDM cosmology is given by

$$P(k) \propto T^2(k)k. \quad (4)$$

The WDM spectrum is truncated at small scales as described by Bode, Ostriker & Turok (2001) through an additional factor in the transfer function of the CDM spectrum such that

¹ A small reduction would occur since concentration of baryonic material forces a moderate increase of the central dark matter density by purely gravitational processes over what would have been the case without efficient baryonic cooling.

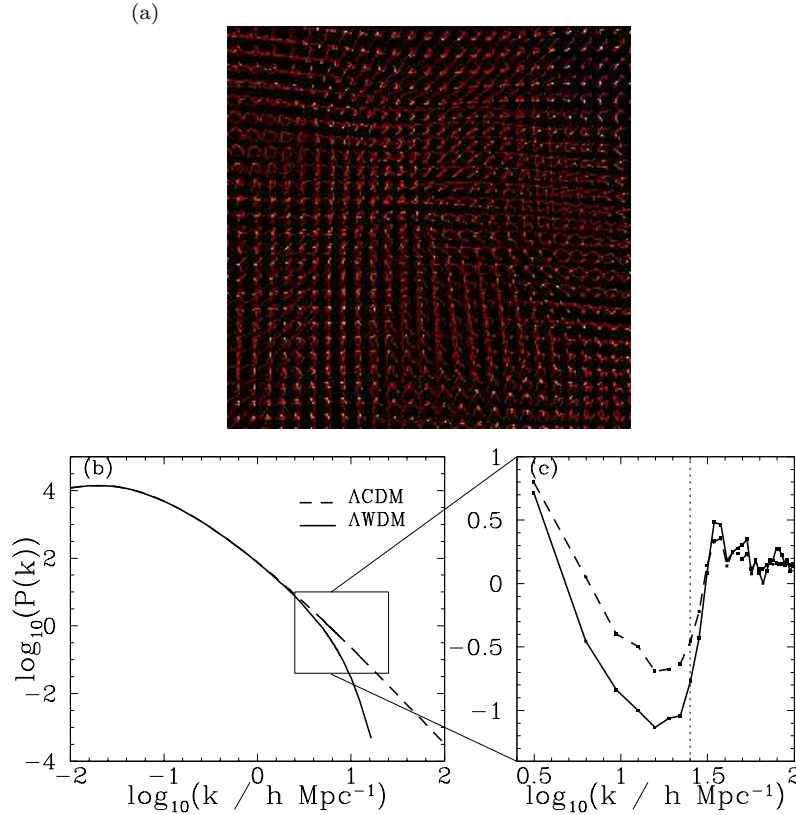


Figure 1. (a) The particle distribution of the Λ WDM simulation initial conditions. (b) A comparison between the input 3-D power spectrum for the Λ CDM cosmology and a warm dark matter power spectrum with particle mass, $m_x = 1.0$ keV. (c) The calculated 3-D power spectrum from the initial conditions of the Λ CDM and Λ WDM simulations. The dotted line is the Nyquist frequency of the particle grid in the case of the 50^3 particle simulations and is also the wavenumber at which noise dominates the spectrum as a result of the discrete nature of the initial conditions. We note that the Λ WDM power spectrum has a cut off which occurs at wave-numbers lower than this numerical limit.

$$T_{\text{WDM}}(k) = \frac{1}{[1 + (\frac{k}{k_{\text{cut}}})^2]^5}, \quad (5)$$

with k_{cut} given by Equation 1. Here, m_x is the mass of the warm dark matter particle which is set to 1 keV as described in the Introduction. The Λ WDM power spectrum $P(k)$ therefore takes the following form:

$$P(k) \propto T_{\text{WDM}}^2(k) T^2(k) k. \quad (6)$$

The amplitude of the mass fluctuations in both cosmologies is normalised so that the *rms* mass fluctuation in spheres of radius $8h^{-1}\text{Mpc}$ is $\sigma_8=0.86$. This normalization was chosen to match the present day abundances of rich galaxy clusters in this cosmology (Eke et al. 1996) and is somewhat higher than the value deduced from more recent analyses (Pierpaoli et al. 2002, Seljak 2001 and Viana et al. 2002). However, the value of $\sigma_8 = 0.86$ is consistent with the WMAP determination and with weak lensing constraints (Refriger 2003), for our adopted value of the spectral index $n = 1$.

The baryonic fraction is set to $f_b = \Omega_b/\Omega_m=0.17$, consistent with the predictions of primordial nucleosynthesis (Burles & Tytler 1998) and WMAP ($f_b = 0.171 \pm 0.025$) for a Hubble parameter of $h=0.65^2$. Figure 1(a) shows a 2-D

projection of the initial particle positions for our 50^3 simulation in the Λ WDM cosmology. Figs. 1(b) and (c) show the power spectra of the Λ CDM and Λ WDM initial conditions calculated from the particle distributions at $z = 24$. The dotted line in Figure 1 (c) shows the limit of our spatial resolution in the 50^3 simulations. At scales smaller than this limit (to the right of the dotted line) there is no input power and the Poisson noise dominates.

Velocity dispersions were added to the initial conditions of the warm dark matter model according to equations (2a & 2b). Additional velocity dispersions smear out the small-scale perturbations through free-streaming. We have performed simulations both with and without additional velocity dispersions and find only small differences at the very centres of the dark matter haloes (slightly less steep cusps when the velocity dispersions were included). The effects of initial velocity dispersions are unimportant for the simulations described in this paper.

We used identical values of $\Omega_0=0.3$, $\Lambda_0=0.7$ for both the Λ WDM and the Λ CDM simulations. The mass of the warm dark matter corresponds to a mass cut-off of

$$M_{\text{cut}} = 1 \times 10^{10} M_{\odot} \left(\frac{\Omega}{0.3}\right)^{-0.45} \left(\frac{h}{0.65}\right)^{3.9} \left(\frac{m_x}{\text{keV}}\right)^{-3.45} \quad (7)$$

in the Λ WDM simulations. The mass resolution of the 50^3 Λ WDM simulation is already sufficient to correctly repre-

² h is defined such that $H_0=100h \text{ kms}^{-1}\text{Mpc}^{-1}$.

Simulation	Number	ϵ_g (kpc)	ϵ_d (kpc)	v_c (kms $^{-1}$)	m_{dm} ($10^6 M_\odot$)	m_g ($10^6 M_\odot$)
Λ CDM 34^3	5	0.8	1.4	126 – 167	116 – 208	29 – 52
Λ CDM 50^3	1	0.5	0.85	165	66	16
Λ WDM 34^3	5	0.8	1.4	125 – 169	116 – 208	29 – 52
Λ WDM 50^3	1	0.5	0.85	162	66	16

Table 1. Summary of some of the properties of the Λ CDM SPH simulations that have been re-simulated in the Λ WDM cosmology. The first column gives the number of gas particles within the high resolution cube (equal to the number of dark matter particles within this volume). The second column lists the number of simulations at each mass resolution. The third and fourth columns list the Plummer softening parameter for the gas and dark matter particles respectively. The fifth column lists the range of the circular speeds of the dark matter haloes (determined within the virial radius at $z = 0$ from the low resolution AP^3M simulations). The sixth column lists the range of gas particle masses.

sent the input power spectrum above this mass cut-off (see Table 2), thus the distribution of dark matter would not be expected to change in a simulation with still higher resolution. However, this is not true of the Λ CDM simulations, which have no mass cut-off. Higher mass resolution in the Λ CDM would be expected to produce earlier collapse of smaller structures.

2.2 Halo Selection

The initial conditions for our simulations were generated in a two stage process. A low resolution dark matter only simulation of a large computational volume was run until the present day. Haloes were selected from the final output of the simulation to be run at higher resolution including Smooth Particle Hydrodynamics (SPH) to represent a dissipative gas component. The re-simulation of these haloes at higher resolution requires the addition of short wavelength fluctuations missing in the low resolution simulations. In addition particles at large distances are averaged hierarchically to represent the tidal field of the entire computational volume by a manageable number of particles. A full description of the methods used to generate our initial conditions can be found in Weil, Eke & Efstathiou (1998) (see also Navarro, Frenk & White 1997). Here we summarise the specific parameters used for the simulations in this paper.

We ran a low resolution dark matter simulation using the Adaptive Particle-Particle, Particle-Mesh (AP^3M) N-body code of Couchman (1991). For both cosmologies, a cube of $L_{box} = 50$ Mpc containing 128^3 particles was evolved from a redshift of $z = 24$ to the present day. The force law used in the code was a Plummer law with a gravitational softening fixed in comoving coordinates at 7 kpc. Identical random phases were used in both cosmologies so that the same haloes could be simulated at higher resolution enabling direct comparisons to be made. We used a spherical over-density group-finding algorithm (Lacey & Cole 1994) to identify virialised haloes at $z = 0$ with masses in the range of $2 \times 10^{12} M_\odot < M_{halo} < 7 \times 10^{12}$ in a low density environment such that the nearest halo with a mass greater than $7.1 \times 10^{11} M_\odot$ is over 1 Mpc away. If applied to a 50^3 Mpc 3 volume of the real universe our selection procedure would identify intermediate-mass giant field ellipticals or S0 galaxies systems similar to the Sombrero galaxy (M104) rather than late type spirals which are of lower mass, or very bright giant ellipticals which are found in high density regions.

Each target halo was re-simulated at a higher resolution with the inclusion of a gas component. We increased the particle number within a cubic volume at redshift $z = 24$ containing all particles that end up within the virialised region of the halo at $z = 0$. Additional short wavelength perturbations were included to account for the missing small-scale power below the Nyquist frequency of the low resolution simulation. The size of the high resolution cube was of the order of $L_{box} = 5$ kpc. The tidal forces from particles outside the high resolution cube were approximated by increasingly massive particles in 5 nested layers of lower and lower resolution. Gas particles with masses chosen to match the baryonic fraction were added in the high-resolution regions, in the same number and at the same positions as the dark matter particles. Outside the high-resolution regions only dark matter particles were included.

In total we ran 6 simulations from $z = 24$ to $z = 0$ for each of the Λ WDM and Λ CDM cosmologies: Five simulations with 2×34^3 particles (labelled (a) to (e)) and one simulation with 2×50^3 particles within the high resolution cube. The simulations will be referred to as the 34^3 and 50^3 simulations hereafter. At the mass and spatial resolution of the 34^3 runs, it is not possible to resolve the internal structure of a forming galaxy and they are used instead to investigate variations in their global properties. The 50^3 simulations are used to investigate the internal properties of the galaxies in detail.

The simulations were performed with the GRAPESPH code as outlined in Weil et al. (1998) using 5 GRAPE-3A boards (Sugimoto et al. 1990) connected to a Sun Ultra-2 workstation. The evolution of the gas component was followed with SPH including radiative cooling and a simple star formation algorithm: Each gas particle that remains in a collapsing region with a density $\rho_{crit} > 7 \times 10^{-23}$ kg m $^{-3}$ (see Navarro & White 1993; Weil et al. 1998) for longer than a local dynamical time was converted into a star particle. Stellar feedback has been included in some simulations, using somewhat ‘ad hoc’ rules (Sommer-Larsen et al. 2002; Meza et al. 2003; Springel & Hernquist 2003). However, it is clear that these representations are far from realistic. We have therefore chosen to make our simulations as simple as possible and hence stellar feedback is ignored. This makes it easier to compare simulations done at different mass resolutions, and to understand if the properties of the final stellar systems depend on whether the dark matter is warm or cold. Theoretical arguments (see *e.g.* Dekel & Silk 1986; Efstathiou

	a		b		c		d		e	
	Λ CDM	Λ WDM	Λ CDM	Λ WDM	Λ CDM	Λ WDM	Λ CDM	Λ WDM	Λ CDM	Λ WDM
R_{vir}/kpc	350	360	330	330	280	280	280	280	300	310
$M_{DM}(R_{vir})/10^{11}M_{\odot}$	21	22	17	17	10	10	10	11	13	14
$\log_{10}(j_h(R_{vir}))$	3.1	3.1	3.2	3.1	3.3	3.4	3.3	3.3	3.2	3.3
$M_{gal}/10^{10}M_{\odot}$	8.0	8.9	7.3	7.9	7.4	6.1	5.5	6.9	6.3	7.2
$\log_{10}(j_*/\text{kpc kms}^{-1})$	1.7	2.3	2.1	1.2	1.4	1.5	2.6	2.7	2.0	2.2

Table 2. The virial radii, virial masses, galaxy masses and specific angular momenta of the galaxies (measured in $\text{kms}^{-1} \text{kpc}$) and dark matter haloes for each of our five, 34^3 simulations in the Λ CDM and Λ WDM simulations at $z=0$. The difference between the cold and warm dark matter simulations are not statistically significant at the gross, integrated level shown in this table.

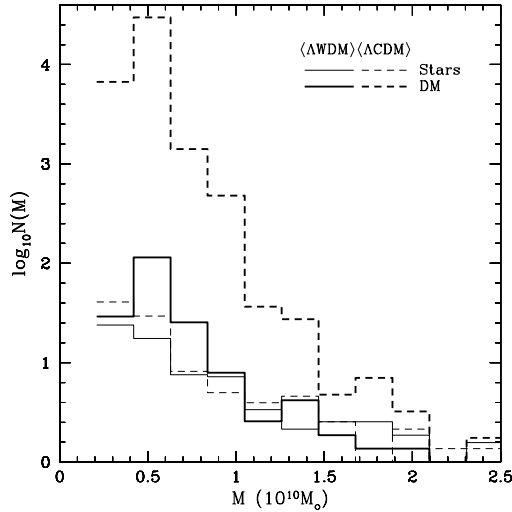


Figure 2. The number of groups (averaged over the 5 simulations) of a given mass in the 34^3 Λ WDM (solid) and Λ CDM (dashed) simulations for both dark matter (thick) and stars (thin) at $z = 0$.

2000) suggest that stellar feedback is less important in high velocity dispersion systems than in low velocity dispersion systems, though since galaxies form hierarchically, feedback processes may have a significant effect on the evolution of high velocity dispersion systems at early times.

3 Λ CDM VS. Λ WDM

3.1 34^3 Simulations

For the Λ WDM cosmology investigated in this paper the formation of halos with masses $M_{halo} < M_{cut} \simeq 1 \times 10^{10} M_{\odot}$ should be suppressed because the initial power spectrum is truncated below this mass-scale. To quantify this effect, we compared the mass spectrum of satellite halos in the two cosmologies at the present day. A friends-of-friends group finding algorithm with a linking length of 0.8 kpc was used to identify dark matter haloes and their stellar systems for

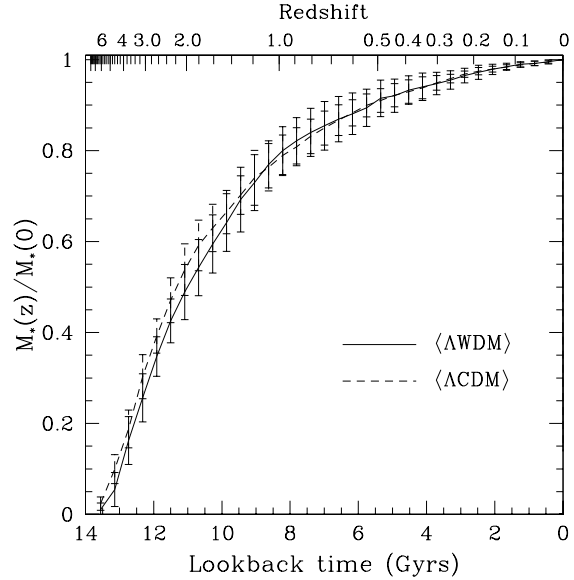


Figure 3. Normalised stellar mass of the central object versus lookback time, averaged over the 5 simulations in the Λ CDM (dashed) and Λ WDM simulations (solid). The error bars indicate the one sigma error. On average the Λ CDM galaxy assembles its stars earlier than the Λ WDM galaxy.

the 34^3 simulations at $z = 0$. The massive central galaxy was excluded.

Figure 2 shows the mass distributions of the dark matter and stellar systems averaged over the 5 simulations in each cosmology. As expected, the Λ CDM cosmology produces many more dark matter haloes with masses $\leq 1 \times 10^{10} M_{\odot}$. There is, however, only a marginal difference in the mass distribution of the stellar systems. The central galaxies in the 34^3 simulations have halo masses in the range of $1.0 \times 10^{12} M_{\odot}$ to $2.2 \times 10^{12} M_{\odot}$, well above the cut-off mass of the Λ WDM cosmology. Table 2 summarizes some of the global properties of the Λ CDM galaxies are their Λ WDM counterpart. The virial radii, masses and the specific angular momenta of the galaxies and their halos do not reveal any large differences between the cold and warm dark matter simulations.

A comparison of the assembly history of the stellar mass

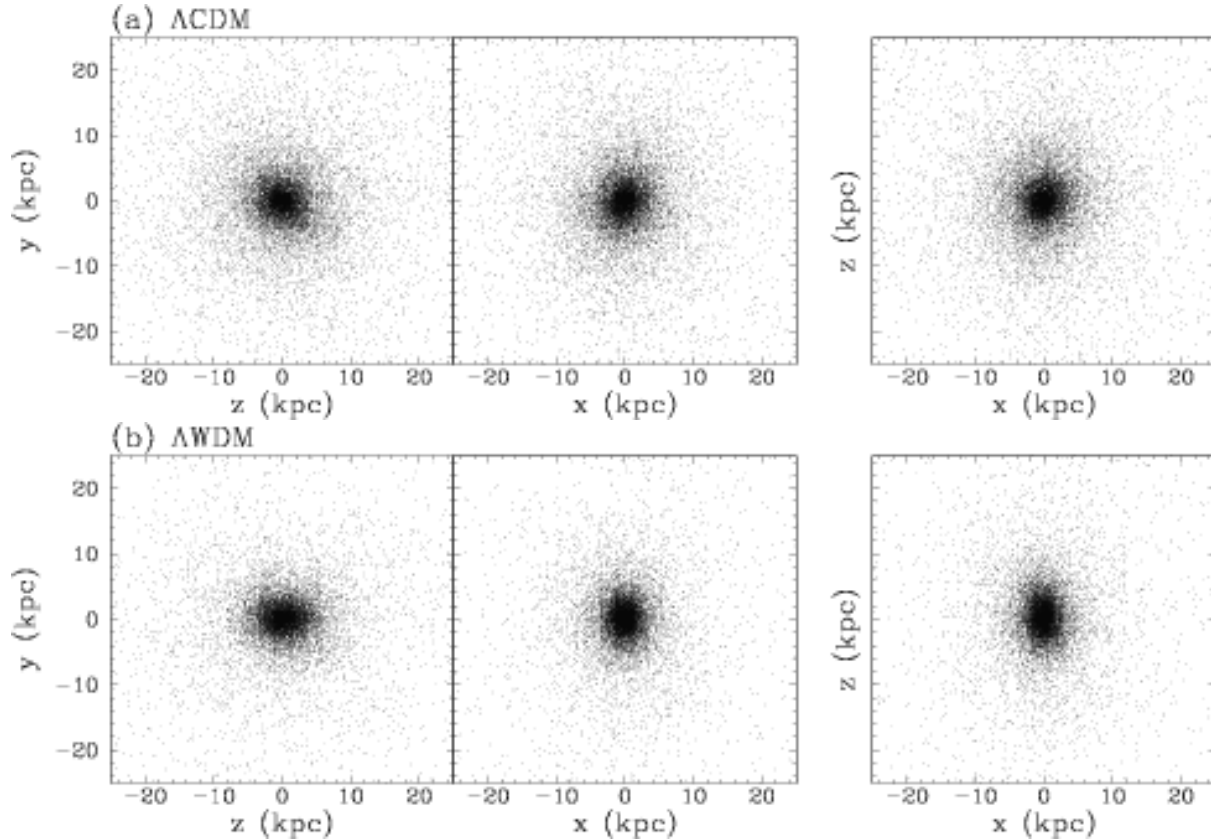


Figure 4. Three orthogonal projections of the star particle positions of the (a) Λ CDM and (b) Λ WDM galaxy in the 50^3 simulations, at $z=0$.

for the central Λ CDM and Λ WDM galaxies averaged over the five 34^3 simulations is shown in Figure 3. The mean values and standard deviations are shown. The redshifts at which 1/10 and 1/2 and 9/10 of the present day mass in stars has been assembled are listed in Table 3. Again, there is no obvious difference between the Λ CDM and the Λ WDM cosmologies. At $z = 0$ the stellar systems in both cosmologies have mean ages of about 10 *Gyrs*. The masses and ages of the galaxies are thus comparable to those of early type galaxies. In conclusion, despite differences in the formation of low mass dark matter haloes, the massive central galaxies formed in the two cosmologies resemble early type galaxies and have indistinguishable formation histories and global properties. The resolution of the 34^3 simulations, however, is too low to investigate the internal properties of the main stellar systems in detail. We therefore now turn to the higher resolution 50^3 simulations.

3.2 50^3 simulations

We have re-simulated halo ‘a’ (see Table 2) using 2×50^3 particles within the high resolution region. Figure 4 shows the three orthogonal projections along the principal axes of the moment of inertia tensor of the central stellar systems in the Λ CDM and Λ WDM cosmologies at $z = 0$. The Λ CDM simulation produces a spheroidal stellar distribution. The Λ WDM galaxy on the other hand has a slightly more flattened morphology. We assume for a moment that the galaxies are two component systems and perform a decomposition

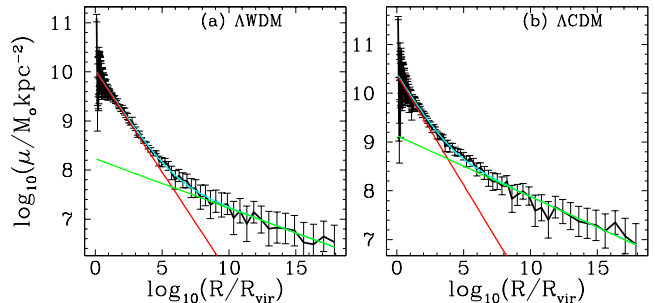


Figure 5. The radial density profile for the galaxies in our 50^3 (a) Λ WDM simulation and (b) Λ CDM simulation. Two exponential fits are also plotted in the figure to represent an inner and outer component. The combined fit is also shown. The best fitting exponentials have been calculated according to Eqn. 8.

of the surface mass density profile into an inner and outer component of the form:

$$\log_{10} \left[\frac{\mu(r)}{\mu_0} \right] = \log_{10} \left[a \exp \left(\frac{-r}{b} \right) + c \exp \left(\frac{-r}{d} \right) \right], \quad (8)$$

where the constants a, b, c and d were determined using a non-linear fitting algorithm. The surface density profiles and the fits for the two galaxies are shown in Figure 5. The stellar system that forms in the Λ WDM simulations has a more extended outer component. More interestingly, however, we see that the inner component of the galaxy in the Λ WDM

simulation is more extended than in the Λ CDM galaxy. To test for evidence of whether the inner and outer components have kinematic counterparts, we performed a kinematic decomposition of the stars. We used a weak criterion to separate a kinematically cold component from a hot component. A star was tagged as a member of a cold component if

$$v_{\theta,i} > 0.7v_c \quad (9a)$$

$$v_{\theta,i} > 2\langle v_{rand}^2 \rangle_i^{1/2} \quad (9b)$$

$$\langle v_{rand}^2 \rangle = \frac{1}{3}(v_{r,i}^2 + (v_{\theta,bin} - \overline{v_{\theta,i}})^2 + v_{z,i}^2) \quad (9c)$$

where v_c is the average circular velocity of the radial bin containing the star, $v_{r,i}$ is the radial velocity of the star, $v_{\theta,i}$ is the rotational velocity of the star, $v_{z,i}$ is the velocity along the minor axis defined by the moment of inertia tensor and $\overline{v_{\theta,bin}}$ is the average rotational velocity of the radial bin containing the star. Both galaxies are essentially hot stellar systems with no significant indication of a dynamically cold sub-component. The Λ WDM galaxy contains a small number of particles which obey the criteria given in equations 9a - 9c which are, however, distributed in a thick disk-like structure.

To quantify whether the flattening of the Λ WDM galaxy is caused by rotation, we have calculated the dimensionless spin parameter, λ , for the dark matter halos and the stellar systems where λ is defined as

$$\lambda = \frac{J|E|^{1/2}}{GM^{5/2}}, \quad (10)$$

and J is the angular momentum, E is the total energy and M is the total mass of the system (see *e.g.* Fall & Efstathiou (1980)). To compute (10) only bound halo particles inside the virial radius and bound stars within the outer radius of the luminous part of the galaxy are included (defined as the radius at which the stellar density of the galaxy averaged in spherical shells becomes equal to the background level). The stellar system is treated as if it were virialised and so $|E|$ in Eqn. 10 is replaced by the kinetic energy of the stars $|T_*|$. In the Λ CDM cosmology the halo has $\lambda_H=0.041$ and the stars have $\lambda_*=0.053$, in the Λ WDM cosmology the halo has a slightly lower value of $\lambda_H=0.032$ whereas the stars have higher value of $\lambda_*=0.228$. Fig. 6 shows the specific angular momentum profiles for the Λ CDM and the Λ WDM galaxy. Neither cosmology produces a purely rotationally supported stellar system ($j_*(r)/j_c(r) \approx 1$, where $j_c(r) = rv_c(r)$ is the specific angular momentum computed from the circular speed). However, the stellar system of the Λ WDM galaxy has a higher angular momentum than the Λ CDM galaxy except in the central regions $r \lesssim 1 \text{ kpc}$.

Figure 7 shows the time evolution of the average specific angular momentum of the dark matter and stars in both cosmologies. At any given redshift the dark matter halo of the Λ CDM galaxy has more angular momentum than the Λ WDM halo, but they both show a very similar evolution with time. In contrast, the angular momentum of the stars of the Λ CDM galaxy does not change significantly after a redshift of $z = 4$ whereas the stars of the Λ WDM galaxy gain further angular momentum until $z = 1$ with little evolution thereafter.

We have investigated the merger histories of the galaxies in more detail. A friends-of-friends algorithm with a linking

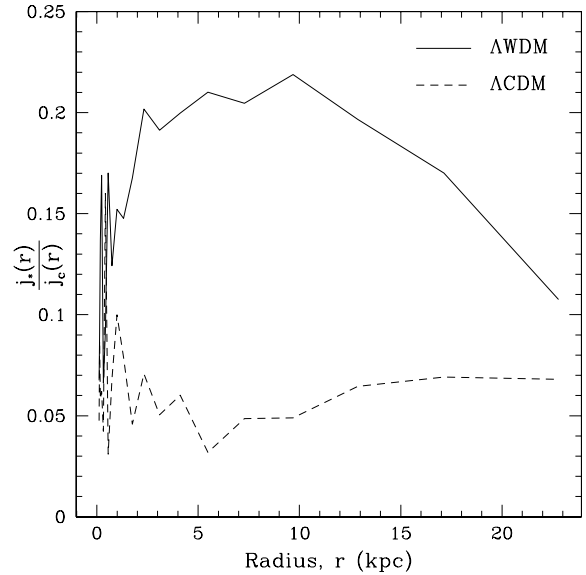


Figure 6. The radial profile of the stellar specific angular momentum as a fraction of the specific angular momentum calculated from the circular velocity. The main stellar system in the Λ CDM (dashed) cosmology has only weak rotational support. The Λ WDM (solid) galaxy has more angular momentum in the outer regions.

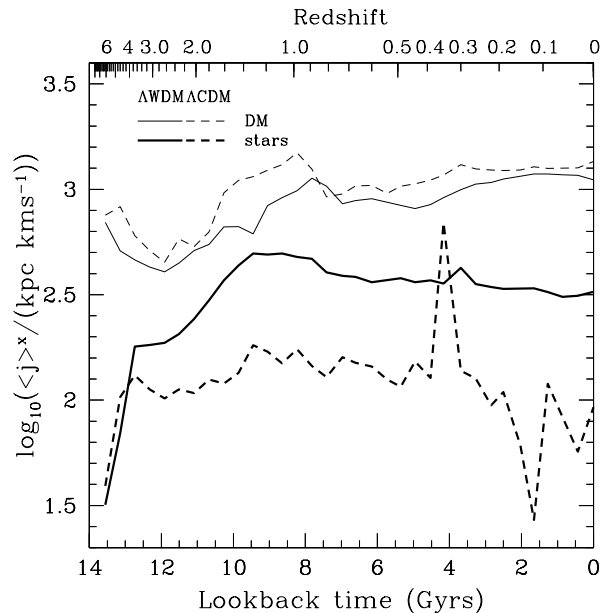


Figure 7. The evolution of the specific angular momentum of stars (thick) and dark matter (thin) for the Λ CDM (dashed) and Λ WDM (solid) galaxy.

length of 2.0 kpc ($\gtrsim 2\epsilon$) was used to identify satellite galaxies consisting of more than 20 stellar particles ($3.2 \times 10^8 M_\odot$) at each redshift. A satellite was then defined to have merged with the central galaxy at a redshift at which its particles were first identified as members of the central galaxy. Figure 8 shows the stellar mass ratio of every identified merger as a

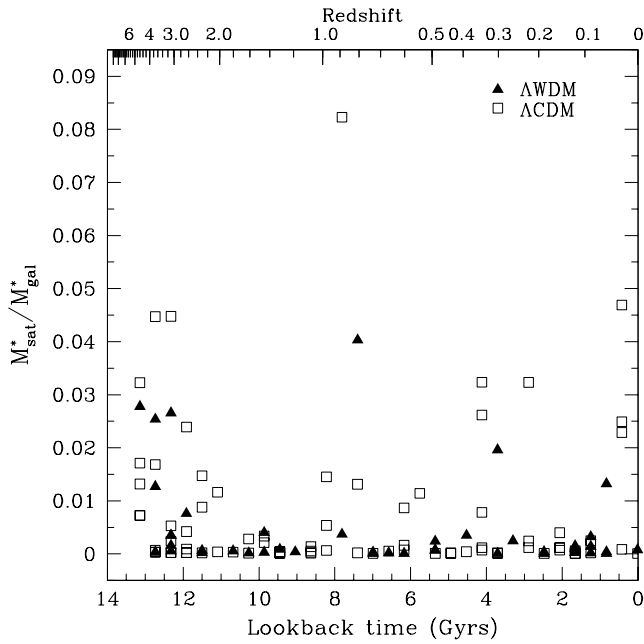


Figure 8. Ratio of the stellar mass of satellites that merge with the central galaxy to the stellar mass of the galaxy as a function of lookback time for both the Λ CDM (open squares) and Λ WDM (filled triangles) cosmology. Every identified satellite with a mass larger than $3.2 \times 10^{18} M_{\odot}$ is plotted.

function of lookback time. The total number of mergers with $M_{\text{sat}}^* > 10^9 M_{\odot}$ is 58 in the Λ WDM simulation compared with 96 in the Λ CDM simulation. The results show that at almost every redshift the Λ CDM galaxy experiences more individual minor mergers with higher mass ratios in stars than the corresponding Λ WDM galaxy. The mass ratio for an individual merger never exceeds 10:1. Low accretion rates like this are expected as the initial conditions were selected from low density environments. In addition to the frequency of mergers, the average internal composition of the merging satellites changes with time and is different in the two cosmologies (Figure 9). At redshifts $z < 2$ the Λ CDM satellites always have a higher star-to-gas ratio. Interestingly, the only redshift range where the satellites have more mass in gas than in stars is $2 < z < 1$. This corresponds to the period where the galaxies reach their second peak in the gas-to-star mass ratios as shown in Figure 10. In this figure we plot the time evolution of the composition of the central galaxy. The mass-ratios of gas to stars (top) and dark matter to stars (bottom) in the Λ WDM and Λ CDM galaxies are plotted. The dark matter fractions vary only slightly between the two cosmologies. However, between a redshift of $z = 4$ and $z = 1$ the Λ WDM galaxy is significantly more gas rich than the Λ CDM galaxy.

To investigate where the stars that end up in the final galaxies have formed, we have calculated the stellar mass accumulated by the galaxies through mergers and compared it to the cumulative mass of stars that formed inside the galaxies (Figure 11). Below a redshift of two, when both galaxies have already assembled $\approx 50\%$ of their final stellar mass (see Figure 16), about 30% of all present day stars in the Λ CDM galaxy have been accreted by mergers and

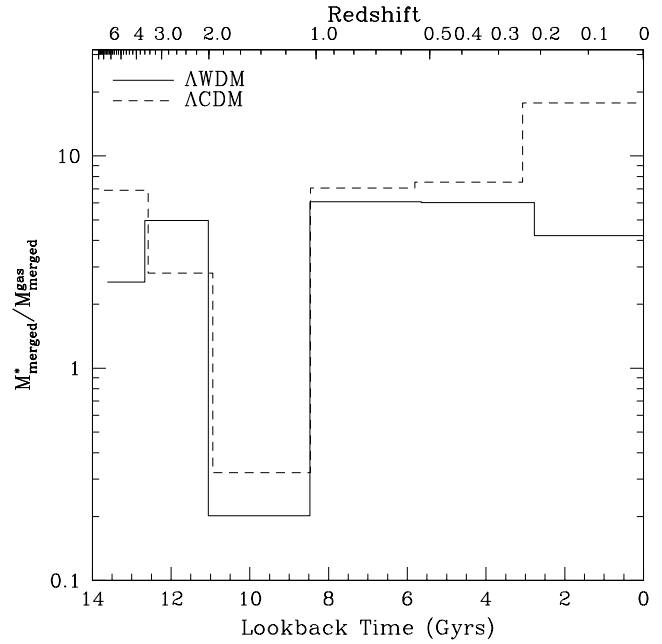


Figure 9. The star to gas mass-ratios of merged satellites as a function of lookback time for the Λ WDM (solid) and Λ CDM (dashed) simulations. Satellites merging at $z < 1$ are in general more gas rich than Λ CDM satellites.

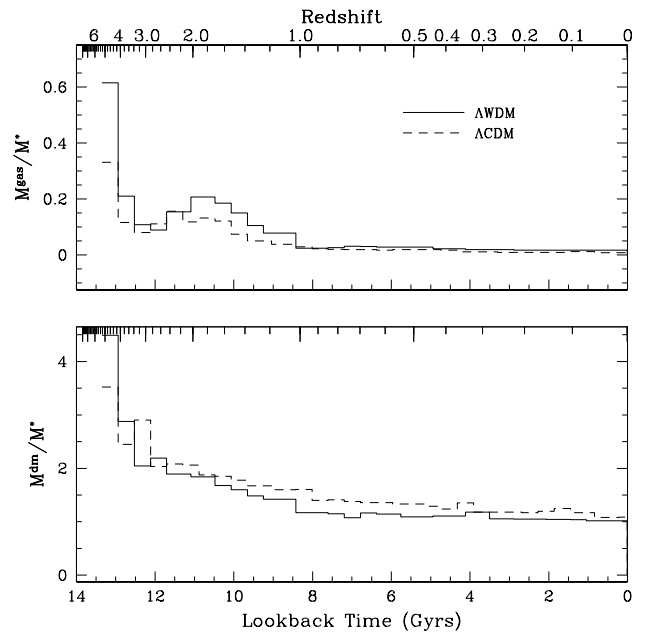


Figure 10. The time evolution of the mass-ratio of gas to stars (top) and dark matter to stars (bottom) of the Λ WDM (solid) and Λ CDM (dashed) galaxies. Throughout the evolution the Λ WDM galaxy is more gas rich than the Λ CDM galaxy.

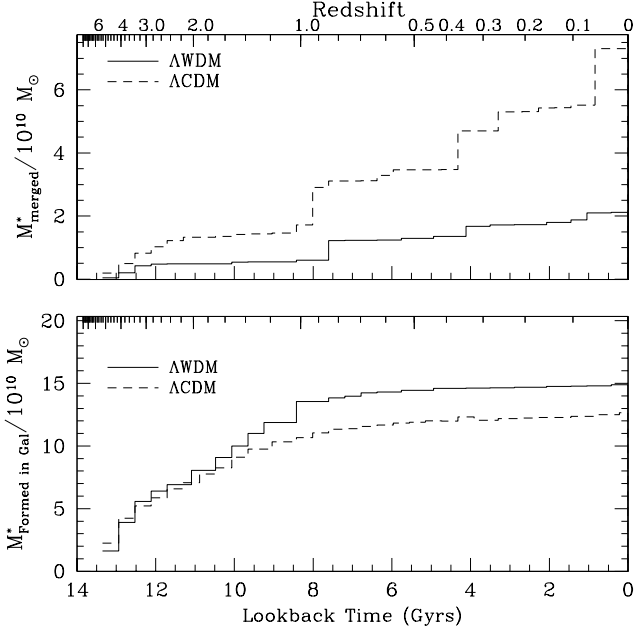


Figure 11. Top: The cumulative stellar mass accreted in mergers as a function of lookback time for the Λ WDM galaxy (solid) and the Λ CDM galaxy (dashed). **Bottom:** The evolution of the stellar mass formed within the galaxies. The masses include material inside a radius of 20 kpc. After $z = 2$ the galaxy in the Λ WDM simulation accretes fewer stars from mergers and interactions and forms the majority of its new stars within the galaxy itself. The Λ CDM galaxy, however, accretes nearly half its mass in stellar mergers.

$\approx 20\%$ of the stars have formed inside the galaxy. Over the same period, the Λ CDM galaxy has accreted only $\approx 10\%$ of its present day stars and $\approx 40\%$ have formed within the galaxy.

The influence of the different accretion histories on the mean ages of the stellar population of the galaxies is shown in Figure 12. In each redshift bin we show the average age of the total stellar population for the Λ CDM (open squares) and the Λ WDM (filled squares) galaxies. In addition, the total stellar population was divided into stars that have merged with the galaxy (thick dashed and solid lines) and stars that have formed in the galaxy (thin dashed and solid lines). At all redshifts the Λ CDM galaxy accretes stars that are of a similar age to the galaxy itself. The accreted stars have formed in small halos at the same time as the stars within the main galaxy. In contrast, the stars accreted in the Λ WDM universe below $z = 0.5$ are on average 1 Gyr younger than the stars within the galaxy. In total, however, the number of accreted stars is so small that there is almost no effect on the mean age of the Λ WDM galaxy.

Fig. 13 shows the star formation rate of the main galaxy in the Λ WDM and Λ CDM simulations. The star formation rate of the Λ CDM galaxy can well be approximated by an exponential, $\text{sfr} \propto \exp(-(t - t_0)/\tau)$, with $t_0 = 13.5$ Gyrs and $\tau = 2.4$ Gyrs. The Λ WDM galaxy does not follow an exponential. There is evidence for a second broad peak in the star formation rate around 10 Gyrs ago which is related

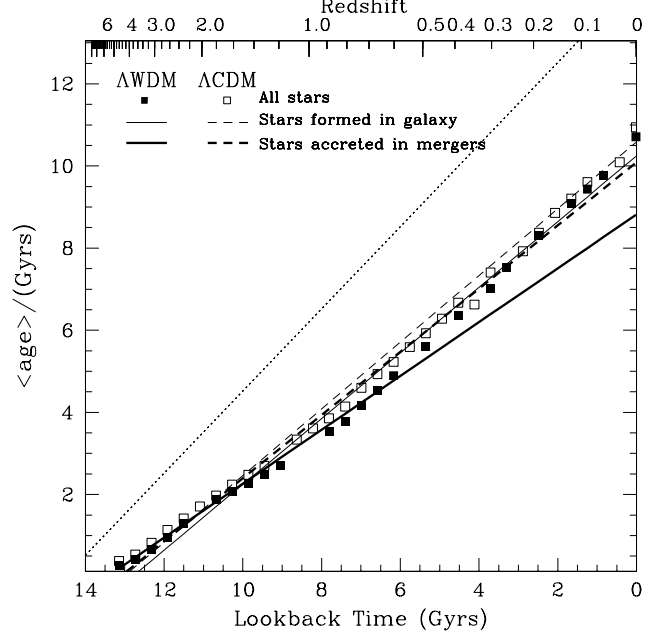


Figure 12. The average age of all the stars within the galaxy in the Λ WDM (filled squares) and Λ CDM (open squares) cosmologies. Linear least squared fits are plotted for the average age of stars formed in the galaxy (thin) and the average age of stars accreted in mergers (thick) for Λ CDM (dashed) and Λ WDM (solid). The dotted line represents the age of the universe. The stellar populations of the mergers in the Λ WDM simulation are on average younger than the corresponding Λ CDM populations. At $z < 1$ there is a difference of approximately 1 Gyr in age.

to the enhanced gas accretion of the Λ WDM galaxy at early times.

The stellar mass assembly history of the 50^3 galaxies is shown in Fig. 16. As for the 34^3 simulations, the early star formation rate of the central galaxy in the Λ WDM cosmology is significantly lower than in the Λ CDM cosmology. Due to this difference in the star formation histories, the Λ CDM galaxy is slightly older (half of its stars are older than 11.9 Gyrs) than the Λ WDM galaxy (half of the stars are older than 11.2 Gyrs).

3.3 Convergence Tests: Anticipated Effect of Extrapolation to Higher Resolution

In this section we investigate the effect of numerical resolution on the global properties of the galaxies formed in the Λ WDM and Λ CDM cosmologies. We estimate the degree to which convergence has been reached by comparing our 34^3 and 50^3 runs, which have identical large scale perturbations.

Table 3 lists some global properties of the 34^3 and 50^3 galaxies. The only value that increases significantly with resolution for both cosmologies is the radius at which the circular velocities reach their peak values. The corresponding circular velocity profiles for the baryonic and dark matter are shown in Fig. 14. The baryonic matter is more concentrated at low resolution. There are a number of possible explanations for this behaviour. If the gas in the inner parts of the galaxy is poorly resolved, star formation leads to a rapid de-

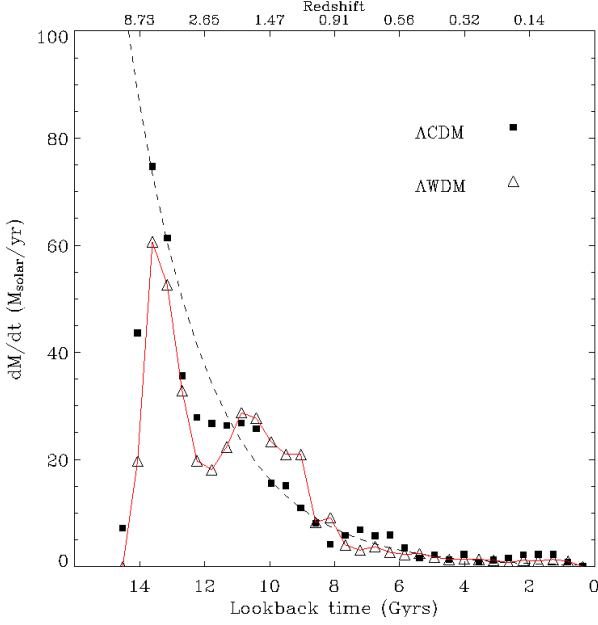


Figure 13. Star formation rate of the ACDM and the Λ WDM galaxy versus lookback time. The evolution of the ACDM galaxy is close to exponential with a star formation rate $\propto \exp(-(t-t_0)/\tau)$ with $t_0 = 13.5$ Gyr and $\tau = 2.4$ Gyr. The Λ WDM galaxy shows a strong peak approx. 13.5 Gyr ago and a broad second peak a little more than 10 Gyr ago.

	ACDM		Λ WDM	
	34^3	50^3	34^3	50^3
$R_{max}^*/(\text{kpc})$	1.0	2.9	1.5	2.7
T_{rot}/T_{rand}	0.006	0.004	0.055	0.064
λ_*	0.046	0.053	0.176	0.228
$M(R_{max}^*)/(10^{10} M_\odot)$	4.49	7.63	6.84	8.43
$\rho^*(R_{max})/(10^{10} M_\odot \text{kpc}^{-3})$	1.09	0.08	0.53	0.11
$(1+z_{1/2}^*)$	3.40	3.62	3.07	3.08
$\log_{10}(\text{Age}^*(R_{max})/\text{yrs})$	9.971	10.01	9.987	10.01

Table 3. The physical parameters of the stellar system formed in our ACDM and Λ WDM simulations at the 34^3 and 50^3 resolution. R_{max}^* is the characteristic radius as calculated from the peak in the circular velocity profile, λ_* is the dimensionless spin parameter for the stars, T_{rot}/T_{rand} is the ratio of the rotational kinetic energy to the energy in random motions, M_* is the total mass within R_{max}^* , $\rho^*(R_{max})$ is the density of the stars within R_{max}^* , $z_{1/2}^*$ is the redshift at which half of the stars have formed and $\text{Age}^*(R_{max})$ is the average age of the stars within R_{max}^* .

pletion of gas resulting in artificial pressure gradients which drive more gas to the center. There is also the possibility that a mismatch of gravitational softening (Plummer) and SPH softening (cubic spline) supports unstable regions to collapse artificially (see Bate & Burkert 1997).

The cumulative mass profile is shown in Fig. 15. The galaxies produced in the 50^3 simulations extend much fur-

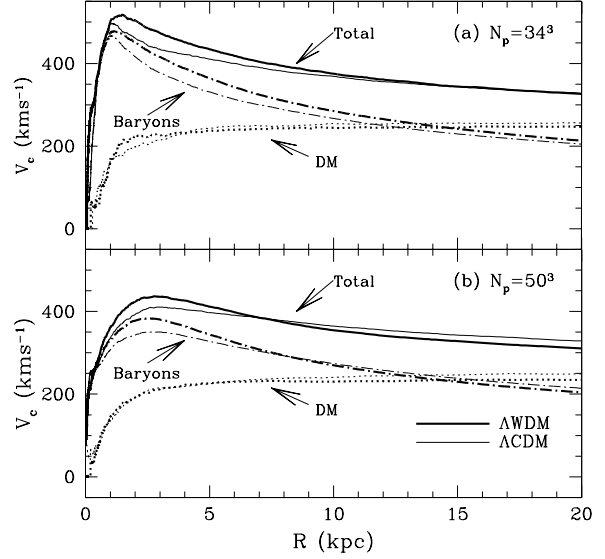


Figure 14. The circular velocity profiles of the 34^3 (upper panel) and 50^3 (lower panel) Λ WDM and ACDM galaxies. The total velocity curves are shown by the solid line. The baryonic (dot-dashed) and dark matter (dotted) contributions are plotted separately. The dynamics of the inner regions ($r < 10$ kpc) is dominated by baryonic material, which is more concentrated at lower resolution, whereas the outer regions of the galaxies are dominated by dark matter.

ther than the lower resolution galaxies due the density criterion that we use to define the size of the galaxy.

Fig. 16 compares the stellar mass within 7 kpc, corresponding to $\approx 2r_{\text{eff}}$, as a function of lookback time for the 34^3 and 50^3 simulations in both cosmologies. We see that the assembly history is resolution dependent for redshifts $z < 2$. The trend goes in opposite directions for the two cosmologies. The Λ WDM galaxy accretes more mass whereas the ACDM galaxy accretes less. The final masses seem to converge at higher resolution. However, we note that our simulations do not include a photo-ionising background which would improve the numerical convergence in the case of the ACDM cosmology.

The collapse of objects smaller than the resolution limit of the simulations is suppressed at early epochs. Thus, when we increase the resolution in the ACDM simulations star formation occurs in objects which did not form at the lower resolution. However, in the power spectrum of the warm dark matter cosmology scales, $\lambda \lesssim 2.5$ Mpc, are intrinsically suppressed. Consequently, we see very little resolution dependence in the star formation history of the Λ WDM simulations as the resolution of the 34^3 simulations is $\lambda = 0.35$ Mpc and therefore well below the cut off in the power spectrum. If we were to increase our resolution still further we would expect that the early star formation in the ACDM simulation to increase whilst very little change would be expected in the history of the Λ WDM simulations.

If we now compare the effect of resolution on the redshift where half of the stars are formed, $z_{1/2}^*$, in the two cosmologies, we see that it increases with resolution in the ACDM cosmology but remains constant for the Λ WDM cosmology

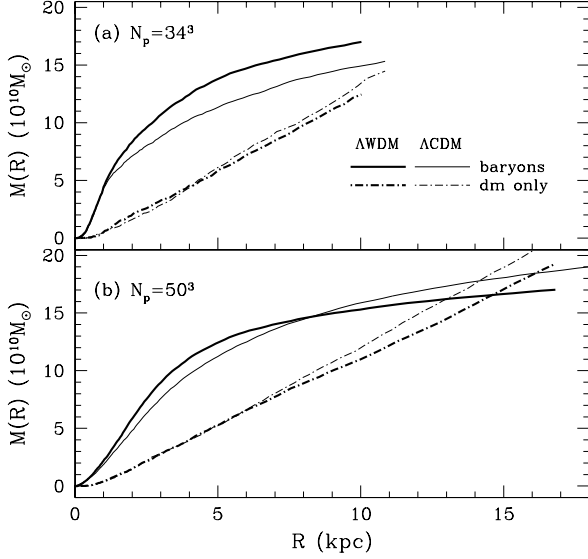


Figure 15. The cumulative mass profiles for the 34^3 (upper panel) and 50^3 (lower panel) ACDM (thick) and Λ CDM (thin) simulations plotted for the dark (dot dashed) and baryonic (solid) matter separately. Within at least 5 effective radii, the galaxies are dominated by dark matter.

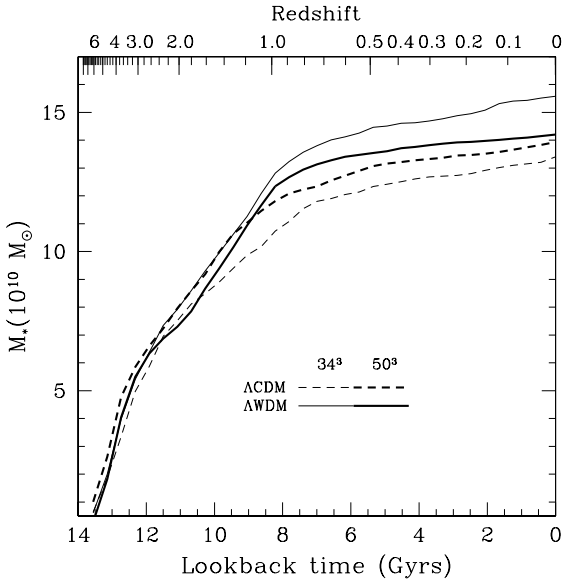


Figure 16. The evolution of stellar mass within 7kpc ($\approx 2r_{\text{eff}}$) for the 34^3 (thin) and 50^3 (thick) simulations in the ACDM (dashed) and Λ CDM (solid) cosmologies. The ACDM simulation appears to have converged by the resolution achieved in the 50^3 simulation, but this is not true of the ACDM simulation.

(Table 3). Thus if we extrapolate to higher resolution we conclude that $z_{1/2}^*$ in the ACDM cosmology will not change but the discrepancy between the formation redshifts in the two cosmologies would increase and could possibly produce a significant observable difference.

4 DETAILED COMPARISON WITH OBSERVATIONS OF ELLIPTICAL GALAXIES

The analysis of the previous sections has shown that the simulated galaxies are hot spheroidal stellar systems. In this section we present a detailed comparison of the two galaxies formed in the 50^3 ACDM and ACDM simulations with observations of giant elliptical galaxies with respect to observed characteristic photometric and kinematical properties, e.g. surface density profile, isophotal deviation from perfect ellipses, velocity dispersion, and major- and minor-axis rotation. In addition we analyse the line-of-sight velocity distribution (LOSVD) of both galaxies. The methods used to analyse the simulated galaxies closely follows the analysis used by observers and is described in detail in Naab & Burkert (2003). Only a brief description will be given here. We created an artificial image of the simulated galaxies by binning the central 35 kpc into 128×128 pixels and smooth it with a Gaussian filter of standard deviation 1.5 pixels. Using this image we derived the surface brightness distribution and the best fitting Sersic-profile (Sersic 1968) $\Sigma = \Sigma_0 \exp(-r^{1/n_{\text{ser}}})$, where n_{ser} is the Sersic-index. For $n_{\text{ser}} = 1$ the profile is exponential, $n_{\text{ser}} = 4$ parameterises the de Vaucouleurs $r^{1/4}$ profile. The isophotes were analysed with respect to the fourth-order cosine deviation, a_4 , from perfect ellipses (Bender et al. 1988). For every projection of a simulated galaxy we defined an effective a_4 -coefficient, $a_{4\text{eff}}$, as the mean value of a_4 between $0.25r_e$ and $1.0r_e$, with r_e being the projected spherical half-light radius. For the moment we are treating (M/L) as constant for all stellar particles regardless of when they were created, or the metallicity of the gas from which they originated.

The characteristic ellipticity ϵ_{eff} for each projection was defined as the isophotal ellipticity at $1.5r_e$. The central velocity dispersion σ_0 was determined as the average projected velocity dispersion of all stellar particles inside a projected galactocentric distance of $0.2r_e$. The characteristic rotational velocity along the major and the minor axis were the projected rotational velocities at $1.5r_e$ and $0.5r_e$, respectively.

We analysed the surface brightness distributions of 100 random projections of the ACDM and ACDM galaxy using the Sersic-profile. The ACDM galaxy has a half-mass radius of $r_{\text{eff}} \approx 3.2\text{ kpc}$ and a mean Sersic-index of $n_{\text{ser}} = 1.8 \pm 0.1$ which is close to the observed lower limit for intermediate-mass ellipticals at the same effective radius (Caon et al. 1993). The ACDM galaxy shows a more exponential profile with a mean Sersic-index of $n_{\text{ser}} = 1.5 \pm 0.15$ at a smaller effective radius of $r_{\text{eff}} \approx 2.2\text{ kpc}$ again consistent with lower observational limits (see Fig. 23). Interestingly, the observed trend for more exponential galaxies to have smaller effective radii is followed. Combined with the ellipticities and isophotal deviations derived in the following section the photometric properties of both galaxies agree with observed ellipticals (see Caon et al. 1993).

In Fig. 17 we show the global analysis of the two galaxies resulting from the 50^3 ACDM (filled boxes) and ACDM (open triangles) simulations seen along 100 random lines-of-sight. The observations of real elliptical galaxies are indicated by plus signs (data kindly provided by Ralf Bender). In the upper left plot of Fig. 17 the projections of the ACDM

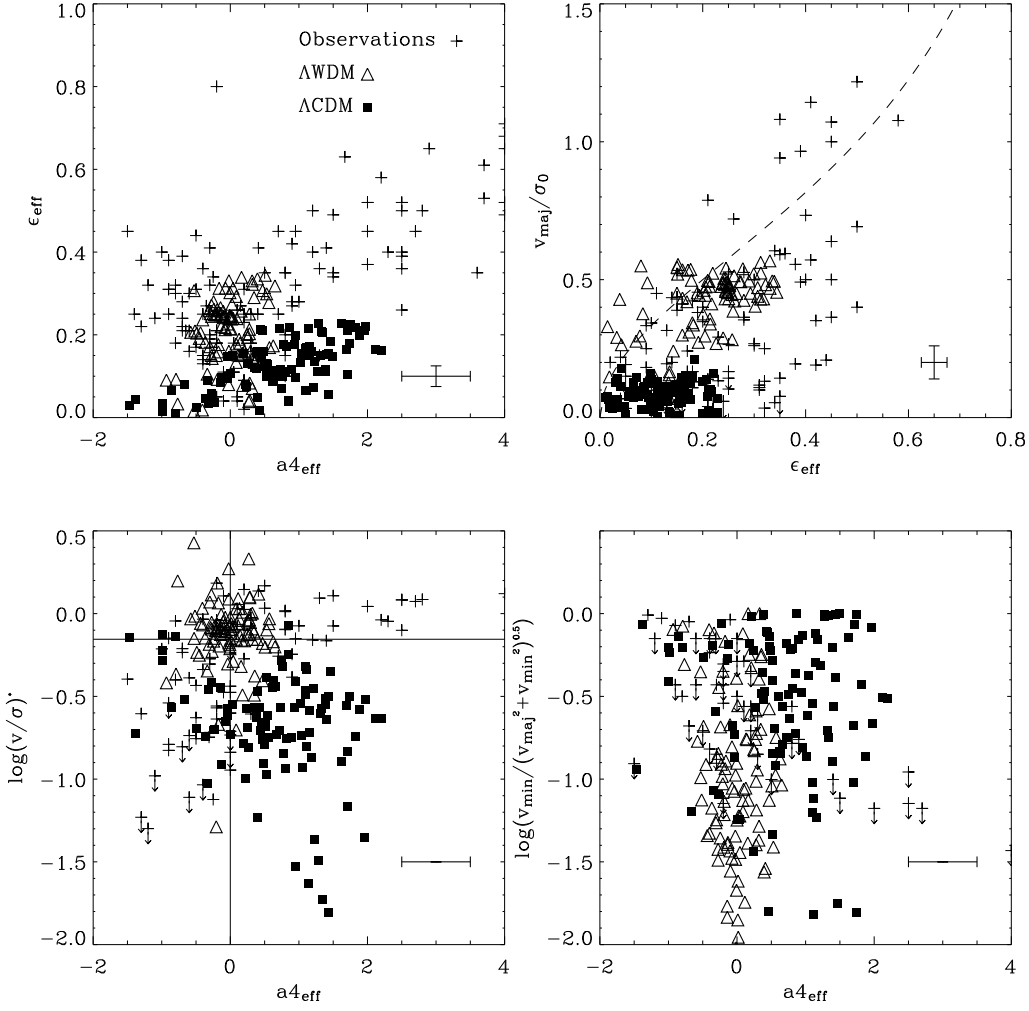


Figure 17. Kinematical and photometric properties for 100 random projections of the simulated Λ WDM and Λ CDM galaxies in the 50^3 simulation. Open triangles show the values for the Λ WDM galaxy while filled boxes indicate the values for the Λ CDM galaxy. Observed values are indicated by plus signs, arrows indicate upper limits (Data kindly provided by Ralf Bender). The errors were derived by statistical bootstrapping. *Upper left panel:* Effective ellipticity ϵ_{eff} of the galaxies versus effective isophotal shape $a4_{\text{eff}}$. *Upper right panel:* Rotational velocity over central velocity dispersion (v_{maj}/σ_0) versus ϵ_{eff} . The dashed line shows the theoretical curve for an oblate isotropic rotator. *Lower left panel:* Anisotropy parameter $(v/\sigma)^*$ versus $a4_{\text{eff}}$. *Lower right panel:* Amount of minor axis rotation versus $a4_{\text{eff}}$ with v_{maj} and v_{min} being the maximum velocity along the major and minor axis, respectively.

galaxy in the $a4_{\text{eff}}-\epsilon_{\text{eff}}$ plane are shown. The galaxy looks almost round with a maximum ellipticity of 0.2 and a peak in the ellipticity distribution around $\epsilon = 0.1$. It has predominantly disk ($a4_{\text{eff}} > 0$) deviations from elliptical isophotes and there is a trend for more disk projections to have higher ellipticities. The Λ WDM galaxy is more elongated and the distribution of ellipticities peaks at $\epsilon = 0.2$ with a maximum of $\epsilon = 0.35$. The isophotes are either slightly boxy or disk. Taking the errors of the a_4 analysis into account the isophotal shape scatters around zero. The area covered by the projections of both galaxies in the $a4_{\text{eff}}-\epsilon_{\text{eff}}$ plane is consistent with the observed distribution. However, the simulations do not reproduce galaxies with $\epsilon_{\text{eff}} > 0$ and $a4_{\text{eff}} > 2$ or $a4_{\text{eff}} < -1$.

With respect to rotation, the Λ CDM galaxy is a slow rotator with $(v_{\text{maj}}/\sigma_0) < 0.2$ (upper right plot in Fig. 17)

and is likely to be flattened by anisotropic velocity dispersions as the anisotropy parameter $(v_{\text{maj}}/\sigma_0)^*$ is in general well below 0.7. As this galaxy shows predominantly disk isophotes it occupies a region in the $(v_{\text{maj}}/\sigma_0)^*-a4_{\text{eff}}$ plane where no real galaxy is observed (lower left plot in Fig. 17). Additionally, in the $(v_{\text{maj}}/\sigma_0)-\epsilon_{\text{eff}}$ -plane the projections cover the area of observed massive boxy ellipticals which are much more luminous than the galaxies presented here. In contrast, the Λ WDM galaxy has projected $(v_{\text{maj}}/\sigma_0)$ -values higher than 0.5, which is consistent with models for rotationally supported galaxies (dashed line in upper right plot of Fig. 17). The galaxy also is fairly isotropic with $(v_{\text{maj}}/\sigma_0)^*$ scattering around zero and agrees well with observed isotropic galaxies with small deviations from elliptical isophotes. None of the projections of the simulated galaxies falls in the area of boxy anisotropic

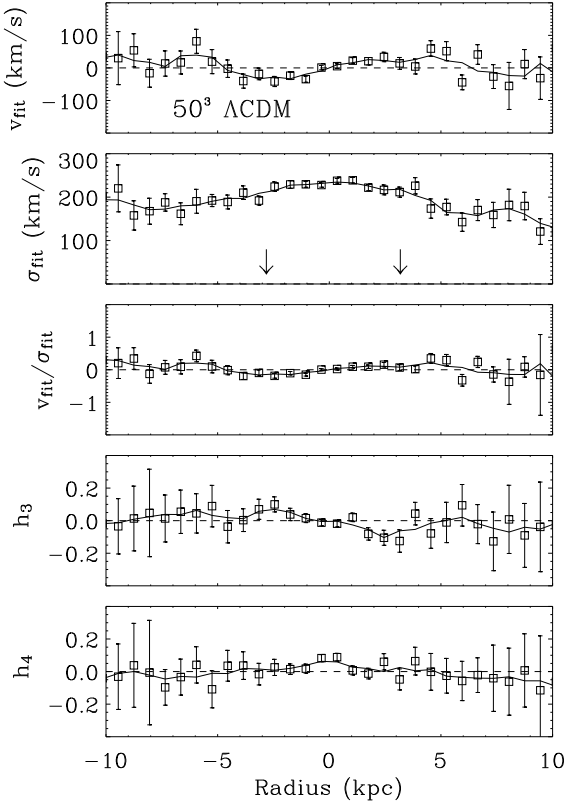


Figure 18. Analysis of the LOSVD of the 50^3 ACDM galaxy as measured along a slit aligned with the major axis of the moment of inertia tensor of the main stellar body (open squares). The fitted local velocity v_{fit} , local velocity dispersion σ_{fit} , $v_{\text{rot}}/\sigma_{\text{fit}}$, h_3 , and h_4 are plotted versus radius. The lines show the smoothed profiles, respectively. The effective radius of the galaxy, $r_{\text{eff}} \approx 3.2$ kpc is indicated by the arrows. The individual error-bars were derived by bootstrapping.

or diskly isotropic ellipticals. Both simulated galaxies show minor-axis rotation (lower right plot of Fig. 17). The ACDM galaxy however disagrees with observations as it shows diskly isophotes at the same time. Observed diskly ellipticals show only weak minor axis rotation.

To analyse the LOSVDs of the simulated galaxies in more detail we placed a slit with a width of 1.5 kpc and a grid spacing of 0.5 kpc along the apparent long axis of each projected remnant. Thereafter all particles falling within each grid cell were binned in velocity along the line-of-sight. The line-of-sight velocity profiles for each bin along the grid were then parameterised by a Gaussian plus third- and fourth-order Gauss-Hermite basis functions (van der Marel & Franx 1993; Bender et al. 1994; Bendo & Barnes 2000). Figs. 18 and 19 show the kinematic parameters (σ_{fit} , v_{fit} , h_3 , h_4) along the long axes of the ACDM and ACDM galaxy, respectively. h_3 and h_4 are the amplitudes of the third- and fourth order Gauss-Hermite functions. For $h_3 = 0$ and $h_4 = 0$ the resulting velocity profile is a Gaussian. For asymmetric profiles with the prograde (leading) wing steeper than the retrograde (trailing) one, h_3 and v_{fit} have opposite signs. When v_{fit} and h_3 have the same sign, the leading wing is broad

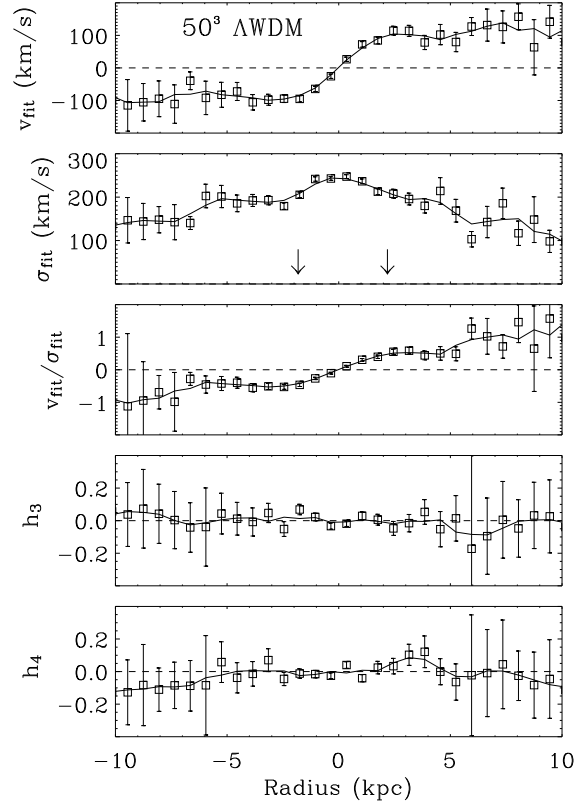


Figure 19. Same as Fig. 18 but for the 50^3 ACDM galaxy. The effective radius of the galaxy, $r_{\text{eff}} \approx 2.2$ kpc is indicated by the arrows.

and the trailing wing is narrow. LOSVDs with $h_4 > 0$ have a 'triangular' or peaked shape, here the distribution's peak is narrow with broad wings. Flat-top LOSVDs have $h_4 < 0$, where the peak is broad and the wings are narrow.

The ACDM galaxy shows very little rotation inside its effective radius (Fig. 18). The velocity dispersion inside r_{eff} is flat and falls off slowly at larger radii therefore $v_{\text{fit}}/\sigma_{\text{fit}}$ never exceeds 0.2. The asymmetry of the LOSVD parameterised by h_3 is anticorrelated with v_{fit} as it is observed for real ellipticals (Bender et al. 1994). The local correlation between h_3 and $v_{\text{fit}}/\sigma_{\text{fit}}$ inside r_{eff} for 100 random projections of the simulated galaxy is shown in upper plot of Fig. 20. h_3 and $v_{\text{fit}}/\sigma_{\text{fit}}$ agree well with observed data (indicated by the shaded area) for $v_{\text{fit}}/\sigma_{\text{fit}} < 0.2$ and are in general anticorrelated. This is also reflected in a negative effective h_3 value, $h_{3\text{eff}}$ (lower plot in Fig. 20) for almost all projections, where $h_{3\text{eff}}$ is defined as the mean value of h_3 inside one effective radius (see Bender et al. 1994). The points follow the observed correlation between $h_{3\text{eff}}$ and v_{rot}/σ_0 .

The ACDM galaxy, as we have already seen in Fig. 17, shows significant rotation (Fig. 19) with the rotation velocity flattening out at around 100 km/s beyond the effective radius. The velocity dispersion profile is more peaked than for the ACDM case. This results in local $v_{\text{fit}}/\sigma_{\text{fit}}$ as high as 0.6. The parameters h_3 and h_4 are consistent with zero inside r_{eff} . Analysed for 100 projections the local value of h_3

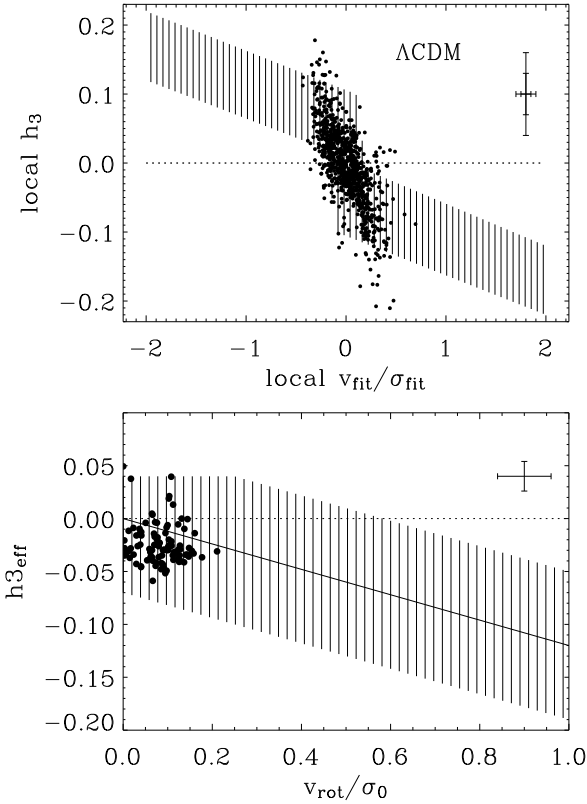


Figure 20. *Upper plot:* Local correlation between h_3 and v_{fit}/σ_0 for the ΛCDM galaxy. The observed data points cover the region indicated by the shaded area. The large error bar indicates the errors for $v_{\text{fit}}/\sigma_0 > 0.2$. *Lower plot:* Global correlation between $h_{3\text{eff}}$ and v_{fit}/σ_0 . The observed correlation (Bender et al. 1994) is shown by a straight line. The maximum spread around this correlation is indicated by the shaded area. The dotted lines indicate the zero line.

does not correlate with $v_{\text{fit}}/\sigma_{\text{fit}}$ which is in contradiction to observations (upper plot of Fig. 21). $h_{3\text{eff}}$ (lower plot in Fig. 21) tends to stay positive and does not follow the observed trend, however it is broadly consistent with observations.

In summary, the ΛWDM galaxy can be interpreted as a modestly rotating isotropic hot stellar system. Its global photometric and kinematical properties are consistent with observations of isotropic ellipticals. The galaxy does, however, not show any strong sign of the fine-structure that would be typical for rotationally supported elliptical galaxies. Its isophotal shape does not deviate significantly from being elliptical and there is no evidence that the LOSVDs show a correlated deviation from a Gaussian. This may be due, at least in part, to an insufficient number of particles in the simulation.

The ΛCDM galaxy shows signatures for being a combined disk/bulge system (except for the very low net rotation rate). The photometric decomposition (Fig. 5) presents evidence for a disk-like sub-component. This is supported by the predominantly disk-like shape of the galaxy. The anticorrelation between h_3 and v/σ provides

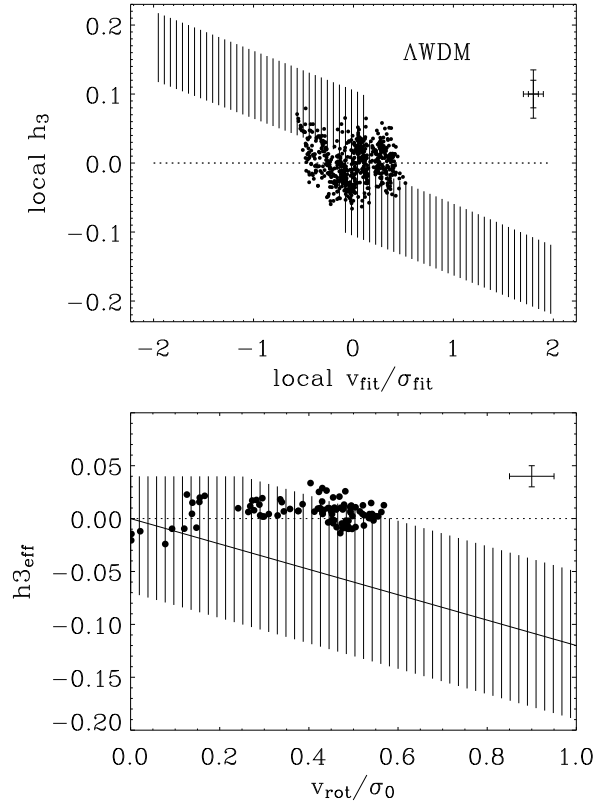


Figure 21. Same as Fig. 20 but for the ΛWDM galaxy.

further kinematical evidence for a combined disk-bulge system (Bender et al. 1994; Naab & Burkert 2001b). From the rotation curves, the round shape and the anisotropic kinematics of the galaxy it becomes clear that the “disk” can contribute only a small fraction to the total mass of the system. However, the ΛCDM galaxy rotates too slowly to be consistent with observations and there is no sign of a disk in the kinematic decomposition. It forms a disk-like system which is not observed.

Due to the uncertain mass-to-light ratios of the simulated galaxies we use the virial theorem to define a dynamical mass $M_{\text{dyn}} = r_{\text{eff}}^2 \sigma_0^2 / G$ using the half-mass radius r_{eff} and the central velocity dispersion σ_0 of every projected galaxy. This mass is used to define a dynamical surface density, $\Sigma_{\text{dyn}} = M_{\text{dyn}}/r_{\text{eff}}^2$, to create a simulated Fundamental Plane where the effective surface brightness SB_e is replaced by Σ_{dyn} . In the same way we derive dynamical masses for observed ellipticals using the observed effective radius and velocity dispersion. Fig. 22 shows a comparison of observed ellipticals with the simulated ΛCDM and ΛWDM galaxies. Both galaxies are consistent with observations. The ΛWDM galaxy has a smaller dynamical mass and has a higher effective surface brightness than the ΛCDM galaxy.

Figure 23 shows a comparison of the mean global projected properties of the simulated galaxies to the global properties of giant elliptical galaxies. The maximum spread in the data and in the observations is indicated by the er-

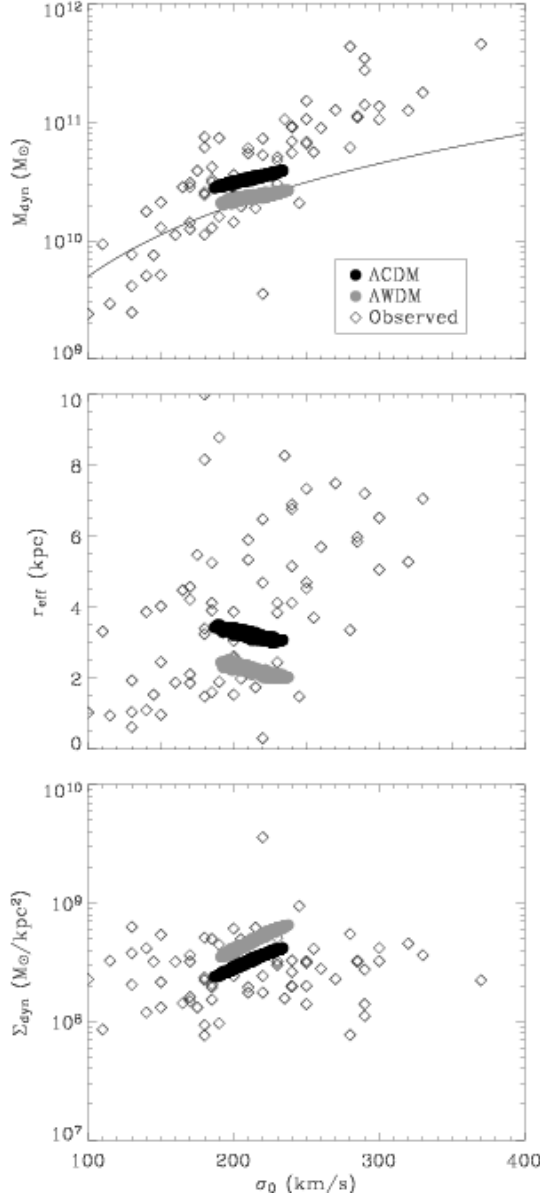


Figure 22. Dynamical mass $M_{\text{dyn}} = r_{\text{eff}}\sigma_0^2/G$, effective radius r_{eff} , and dynamical surface-brightness, Σ_{dyn} , versus central velocity dispersion σ_0 . Black dots represent projections of the ΛCDM , grey dots of the ΛWDM galaxy, respectively. For the simulated galaxies r_{eff} is the projected spherical half-mass radius.

ror bars. It becomes clear from this figure that we produced “ordinary” ellipticals in our simulations which compare very well to the average properties of giant ellipticals.

The low number of stellar particles within the half-mass radii of the simulated galaxies (≈ 7000) makes it too early to draw any final conclusion on the real structure of intermediate mass ellipticals in ΛWDM or ΛCDM cosmologies. Especially as the ΛCDM simulations are not yet numerically converged. Relaxation effects in particular might significantly influence the dynamics of the systems (see Diemand et al. 2003)

The present resolution is already sufficiently high to perform a kinematical and photometric analysis within reasonable error limits (all errors have been determined by

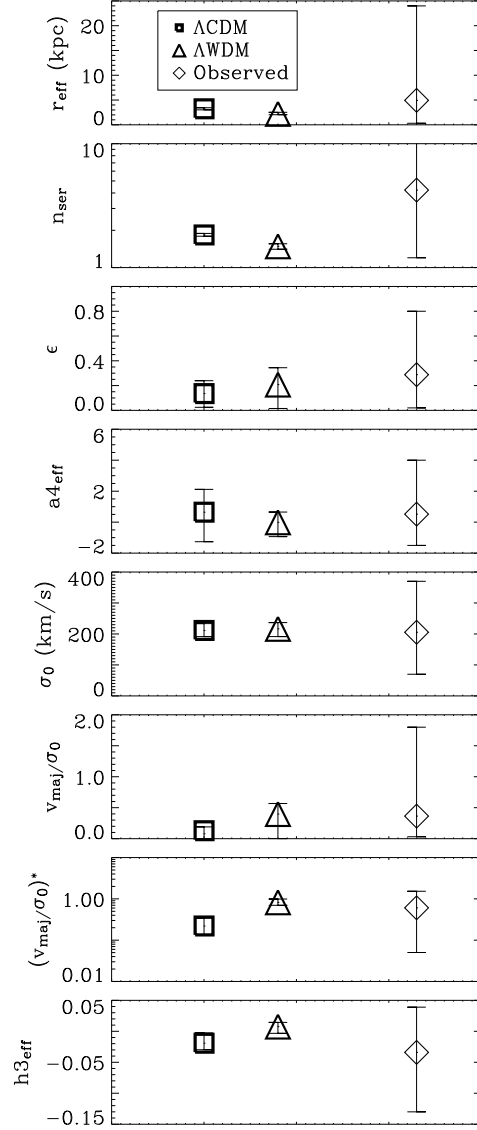


Figure 23. Mean properties of the simulated ΛCDM (squares), ΛWDM (triangles) and observed (diamonds) elliptical galaxies. The maximum spread in the data is indicated by the error bars. For the two simulated galaxies the spread is due to projection effects. Observational data for the effective radius (r_{eff}), ellipticity (ϵ), effective isophotal shape ($a_{4\text{eff}}$), rotation velocity (v_{maj}) and velocity dispersion (σ_0) have been kindly provided by Ralf Bender. Data for the Seric index n_{ser} have been taken from Caon et al. (1993) and for the LOSVD asymmetries ($h_{3\text{eff}}$) from Bender et al. (1994).

applying the statistical bootstrapping method (see Heyl et al. 1994) both for global and local measurements (see e.g. Figs. 17, 18). Therefore we are able to trace the real structure of the simulated galaxies at the present resolution. Increasing the resolution, however, will very likely change the detailed internal stellar structure of the simulated galaxies whereas the differences will presumably be stronger for ΛCDM (as we have shown in the previous section) than for ΛWDM cosmologies. A preliminary analysis of a higher

resolution Λ CDM supports this conclusion.

5 CONCLUSIONS

We have presented the results of ten 34^3 particles and two 50^3 particles simulations of the formation of individual galaxies in a warm and cold dark matter cosmology with a cosmological constant. The sample of low resolution simulations enabled us to compare the global properties of the dark matter haloes and galaxies formed in the two different cosmologies. The two galaxies selected for re-simulation reside in a low density environment. Consequently the models presented here are likely to trace the formation of ordinary intermediate mass giant elliptical or S0/Sa galaxies in the field, for example, the Sombrero galaxy (M104). The two high resolution simulations have been used to investigate the assembly histories of the final galaxies and to compare their internal properties with those of real early type galaxies.

As expected from the suppression of small-scale structure in the initial conditions, the Λ WDM cosmology produces fewer low mass dark matter haloes ($M_{halo} < 10^{10} M_{\odot}$) at the present epoch compared with the Λ CDM cosmology (Bode et al. 2001). This feature is also reflected in the assembly histories of the two 50^3 simulations. At almost all redshifts, the Λ CDM galaxy experiences more minor mergers with higher mass-ratios (up to 10:1) than the corresponding Λ WDM galaxy. Low accretion rates, and the absence of any major merger event, are expected since the initial conditions were selected from low density environments. In addition to differences in the frequency of mergers, the internal composition of the merging satellites differs in the two cosmologies. The Λ WDM satellites are always more gas rich. At redshifts $z < 0.3$ the star-to-gas ratio is about an order of magnitude higher in the Λ CDM than in the Λ WDM cosmology. As a result, below a redshift of two (when both galaxies have already assembled $\approx 50\%$ of their final stellar mass) about 30% of all present day stars in the Λ CDM galaxy have been accreted by mergers and $\approx 20\%$ of the stars have formed inside the galaxy. Over the same period the Λ WDM has accreted only $\approx 10\%$ of its present day stars and $\approx 40\%$ have formed within the galaxy.

A further difference between the two cosmologies is evident in the angular momentum evolution of the galaxies. The halo of the Λ CDM galaxy has higher angular momentum than the Λ WDM halo but they both show a similar temporal evolution. In contrast, the average angular momentum of the stars of the Λ CDM galaxies does not change significantly after a redshift of $z = 4$ whereas the stars of the Λ WDM galaxy gain further angular momentum until $z = 1$, with little evolution thereafter. Between a redshift of $z = 4$ and $z = 1$ the Λ WDM galaxy is more gas rich and forms more stars within the galaxy than its Λ CDM counterpart, resulting in a second peak in the star formation rate at $z \approx 1.5$.

We conclude that the removal of small scale power reduces the frequency of mergers. The reduction in the number of massive sub-halo mergers in the 50^3 warm dark matter simulation produces a galaxy with significantly higher angular momentum at $z=0$. The increase in the specific angular momentum of objects in the warm dark matter simulations

suppresses the collapse of gas within the simulations, which in turn reduces the star formation rate of the central galaxy at early epochs.

We performed a photometric and kinematical decomposition of the main stellar systems in the 50^3 simulations. Both galaxies are dominated by a hot spheroidal component. The global projected properties of the two 50^3 Λ CDM and Λ WDM galaxies resemble those of real elliptical galaxies. The total masses, density profiles, effective radii, ellipticities, global values of isophotal shapes and LOSVD asymmetries are consistent with the average global properties of giant elliptical galaxies of intermediate masses. This is in contrast to properties of very massive, anisotropic, and boxy ellipticals with large effective radii, typically found in clusters of galaxies. As the physical properties of massive ellipticals differ from those of ordinary intermediate mass ellipticals with respect to inner density-profiles, sizes, isophotal shapes and X-ray and radio properties (Bender et al. 1989; Caon et al. 1993; Faber et al. 1997), we can conclude that they must have formed in a denser environment and, therefore had different formation histories.

Investigating the Λ WDM galaxy in detail revealed that it appears to be an isotropic fast rotator with only weak fine structure both in its isophotal shape (the isophotes are elliptical) and in its LOSVDs (which on average have a Gaussian shape). The ratio of T_{rot}/T_{rand} is a factor of ten higher for the Λ WDM than for the Λ CDM system. Observed rotationally supported ellipticals with similar rotational support do, however, show on average stronger asymmetries in their LOSVDs. The detailed photometric and global kinematical properties do agree very well with observations. The half-mass radius of stellar population is 2.3 kpc . In contrast, the Λ CDM galaxy shows only weak rotation and appears to have anisotropic velocity dispersions. The isophotes are predominantly disk and the LOSVDs show the observed trend which indicates the presence of a weak disk component embedded in the spheroidal body of the galaxy (Rix & White 1990; Bender et al. 1994; Naab & Burkert 2001b). However, anisotropic disk systems, like the Λ CDM elliptical, are in general not observed. The half-mass radius of the Λ CDM galaxy is 3.2 kpc . The mean age of the stellar population of both galaxies is about 10 Gyr s which is in good agreement with the ages of early type galaxies.

Meza et al. (2003) have recently simulated the formation of an individual elliptical galaxy in a Λ CDM cosmology which is only a little more massive (by a factor of about 1.5) than our Λ CDM galaxy. However, their galaxy does not match the global properties of observed giant ellipticals as its stellar distribution is far too dense. Numerical resolution is unlikely to cause the difference as their initial particle masses and softening lengths are comparable to the values used for the simulations presented here. Their final galaxy, however, has significantly more stellar particles (≈ 65000) than our galaxies (≈ 13000). This is due to differences in the star formation algorithms. Meza et al. (2003) split their gas particles into several stars which can have different masses. As a result their mean stellar particle mass is a factor of four smaller than our fixed stellar mass. It is not clear in how far this difference influences the results, e.g. due to mass segregation effects in the stellar distribution. A further difference is that Meza et al. (2003) make their stars at a rate proportional to the gas density with a relatively low efficiency.

In the simulations presented here a gas particle is turned into a star particle as soon as its density is above a certain threshold for more than a dynamical time. As a result the gas in the Meza et al. (2003) simulation can collapse to much higher densities before stars are formed.

In addition we omitted feedback processes in our simulations. Meza et al. (2003) implemented thermal and kinematical feedback. Although one might naively expect that the inclusion of feedback would result in less compact objects, this goes in the opposite direction to explain the differences between their results and ours. Another possible explanation for the differences is the merger history. Our galaxies experience only minor mergers with mass ratios up to 10:1. The Meza et al. (2003) galaxy undergoes a late major merger with a mass-ratio of 3:1 which could effectively drive gas into the centre and convert it into stars. However, the star formation history is not significantly different from our Λ CDM galaxy which undergoes no major merger. The merger is therefore more likely to influence the dynamics of the system rather than have a major effect on the concentration of the bulk of the stellar population.

Based on the simulations at two different resolutions in a Λ CDM and Λ WDM cosmology it becomes clear that this investigation is not yet definitive. As the simulations are not yet fully numerically resolved (especially the Λ CDM simulation) we cannot say with confidence whether Λ CDM or Λ WDM produces galaxies that most closely resemble real elliptical galaxies. In conclusion, we can state that with the simple physics included in our simulations, it is possible to produce ellipticals in both cosmologies with global properties that are in good agreement with observations of intermediate mass giant ellipticals or S0s. However, the combination of the detailed properties of our simulated galaxies (which are very likely to be resolution dependent), like the shape of the LOSVD or the isophotal shape, differ slightly from observations of real ellipticals for one combination or the other. Future simulations at higher resolution will hopefully enable us to determine which, if either, of the two cosmologies produce galaxies which match the observations.

6 ACKNOWLEDGEMENTS

Thorsten Naab acknowledges the award of a PPARC PDRA.

REFERENCES

- Abadi M. G., Navarro J. F., Steinmetz M., Eke V. R., 2003, *ApJ*, 591, 499
- Bahcall N., Dong F., Bode P., SDSS Collaboration 2002, American Astronomical Society Meeting, 201, 0
- Barkana R., Haiman Z., Ostriker J. P., 2001, *ApJ*, 558, 482
- Barnes J. E., 1988, *ApJ*, 331, 699
- Barnes J. E., 2002, *MNRAS*, 333, 481
- Barnes J. E., Hernquist L., 1996, *ApJ*, 471, 115
- Bate M. R., Burkert A., 1997, *MNRAS*, 288, 1060
- Bender R., Burstein D., Faber S. M., 1992, *ApJ*, 399, 462
- Bender R., Doebereiner S., Moellenhoff C., 1988, *A&AS*, 74, 385
- Bender R., Saglia R. P., Gerhard O. E., 1994, *MNRAS*, 269, 785
- Bender R., Surma P., Doebereiner S., Moellenhoff C., Madejsky R., 1989, *A&A*, 217, 35
- Bendo G. J., Barnes J. E., 2000, *MNRAS*, 316, 315
- Benson A. J., Lacey C. G., Baugh C. M., Cole S., Frenk C. S., 2002, *MNRAS*, 333, 156
- Binney J. J., Evans N. W., 2001, *MNRAS*, 327, L27
- Bode P., Ostriker J. P., Turok N., 2001, *ApJ*, 556, 93
- Burles S., Tytler D., 1998, *ApJ*, 499, 699
- Caon N., Capaccioli M., D'Onofrio M., 1993, *MNRAS*, 265, 1013
- Cen R., 2003, *Astro-Ph*, 0303236
- Chiu W. A., Fan X., Ostriker J. P., 2003, *Astro-Ph*, 0304234
- Colin P., Klypin A., Valenzuela O., Gottlober S., 2003, submitted to *ApJ*, astro-ph/0308348
- Couchman H. M. P., 1991, *ApJ*, 368, L23
- Dekel A., Silk J., 1986, *ApJ*, 303, 39
- Diemand J., Moore B., Stadel J., Kazantzidis S., 2003, submitted to *MNRAS*, astro-ph/0304549
- Dubinski J., Mihos J. C., Hernquist L., 1996, *ApJ*, 462, 576
- Dutton A., Courteau S., Carignan C., de Jong R., 2003, submitted to *AJ*, astro-ph/0310001
- Efstathiou G., 2000, *MNRAS*, 317, 697
- Efstathiou G., Bond J. R., White S. D. M., 1992, *MNRAS*, 258, 1P
- Eke V. R., Cole S., Frenk C. S., Navarro J. F., 1996, *MNRAS*, 281, 703
- Eke V. R., Navarro J. F., Steinmetz M., 2001, *ApJ*, 554, 114
- Faber S. M., Tremaine S., Ajhar E. A., Byun Y., Dressler A., Gebhardt K., Grillmair C., Kormendy J., Lauer T. R., Richstone D., 1997, *AJ*, 114, 1771
- Fall S. M., Efstathiou G., 1980, *MNRAS*, 193, 189
- Governato F., Mayer L., Wadsley J., Gardner J. P., Willman B., Hayashi E., Quinn T., Stadel J., Lake G., 2002, *Astro-Ph*, 0207044
- Hernquist L., 1992, *ApJ*, 400, 460
- Heyl J. S., Hernquist L., Spergel D. N., 1994, *ApJ*, 427, 165
- Klypin A., Kravtsov A. V., Valenzuela O., Prada F., 1999, *ApJ*, 522, 82
- Lacey C., Cole S., 1994, *MNRAS*, 271, 676
- Meza A., Navarro J. F., Steinmetz M., Eke V. R., 2003, *ApJ*, 590, 619
- Mihos J. C., Hernquist L., 1996, *ApJ*, 464, 641
- Moore B., Quinn T., Governato F., Stadel J., Lake G., 1999, *MNRAS*, 310, 1147
- Naab T., Burkert A., 2001a, in ASP Conf. Ser. 230: Galaxy Disks and Disk Galaxies Gas Dynamics and Disk Formation in 3:1 Mergers. pp 451–452
- Naab T., Burkert A., 2001b, *ApJ*, 555, L91
- Naab T., Burkert A., 2003, accepted for publication by *ApJ*, 555, 555
- Navarro J. F., Frenk C. S., White S. D. M., 1995, *MNRAS*, 275, 56
- Navarro J. F., Frenk C. S., White S. D. M., 1997, *ApJ*, 490, 493
- Navarro J. F., Steinmetz M., 1997, *ApJ*, 478, 13
- Navarro J. F., White S. D. M., 1993, *MNRAS*, 265, 271
- Navarro J. F., White S. D. M., 1994, *MNRAS*, 267, 401
- Negroponte J., White S. D. M., 1983, *MNRAS*, 205, 1009
- Percival W. J., Sutherland W., Peacock J. A., Baugh C. M., Bland-Hawthorn J., Bridges T., Cannon R., + 20 Co-authors 2002, *MNRAS*, 337, 1068
- Pierpaoli E., Borgani S., Scott D., White M., 2002, *Astro-Ph*, 10, 116
- Refriger A., 2003, *ARA&Ain press*, astro-ph/0307212
- Ricotti M., 2003, *MNRAS*, 344, 1237
- Rix H., White S. D. M., 1990, *ApJ*, 362, 52
- Seljak U., 2001, *Astro-Ph*, 0111362
- Sersic J. L., 1968, *Atlas de galaxias australes*. Cordoba, Argentina: Observatorio Astronomico, 1968
- Sommer-Larsen J., Götz M., Portinari L., 2002, *Ap&SS*, 281, 519
- Spergel D. N., Verde L., Peiris H. V., Komatsu E., Nolte M. R., Bennett C. L., Halpern M., Hinshaw G., Jarosik N., Kogut

- A., Limon M., Meyer S. S., Page L., Tucker G. S., Weiland J. L., Wollack E. and Wright E. L., 2003, *Astro-Ph*, 0302209
- Springel V., 2000, *MNRAS*, 312, 859
- Springel V., Hernquist L., 2003, *MNRAS*, 339, 289
- Steinmetz M., Navarro J. F., 1999, *ApJ*, 513, 555
- Sugimoto D., Chikada Y., Makino J., Ito T., Ebisuzaki T., Umemura M., 1990, *Nature*, 345, 33
- Thomas D., Maraston C., Bender R., 2002, *Ap&SS*, 281, 371
- van der Marel R. P., Franx M., 1993, *ApJ*, 407, 525
- Viana P. T. P., Nichol R. C., Liddle A. R., 2002, *ApJ*, 569, L75
- Weil M. L., Eke V. R., Efstathiou G., 1998, *MNRAS*, 300, 773
- Weil M. L., Hernquist L., 1996, *ApJ*, 460, 101
- Wright L. J., 2002, *Numerical Simulations of Disc Galaxy Formation*. *PhD Thesis*, University of Cambridge
- Yoshida N., Sokasian A., Hernquist L., Springel V., 2003, *Astro-Ph*, 0303622